General Disclaimer

One or more of the Following Statements may affect this Document

- This document has been reproduced from the best copy furnished by the organizational source. It is being released in the interest of making available as much information as possible.

- This document may contain data, which exceeds the sheet parameters. It was furnished in this condition by the organizational source and is the best copy available.

- This document may contain tone-on-tone or color graphs, charts and/or pictures, which have been reproduced in black and white.

- This document is paginated as submitted by the original source.

- Portions of this document are not fully legible due to the historical nature of some of the material. However, it is the best reproduction available from the original submission.

A DIGITAL TECHNIQUE TO COMPENSATE FOR

TIME-BASE ERROR IN MAGNETIC TAPE RECORDING

by

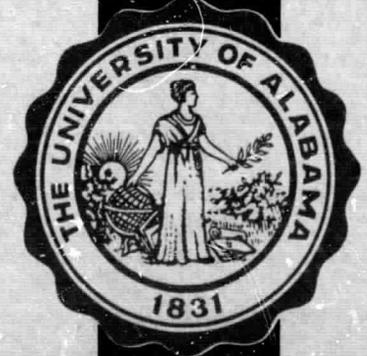RICHARD S. SIMPSON
RONALD C. HOUTS
and
DONALD W. BURLAGE

October, 1968

TECHNICAL REPORT NUMBER 15

SYSTEMS ENGINEERING GROUP

BUREAU OF ENGINEERING RESEARCH

UNIVERSITY OF ALABAMA   UNIVERSITY, ALABAMA

THE UNIVERSITY OF ALABAMA
1831

A DIGITAL TECHNIQUE TO COMPENSATE FOR

TIME-BASE ERROR IN MAGNETIC TAPE RECORDING

by

RICHARD S. SIMPSON
RONALD C. HOUTS
and
DONALD W. BURLAGE

October, 1968

TECHNICAL REPORT NUMBER 15

Prepared for
National Aeronautics and Space Administration
Marshall Space Flight Center
Huntsville, Alabama

Under

Contract Number NAS8-20172

Communication Systems Group
Bureau of Engineering Research
University of Alabama

ABSTRACT

A digital technique is presented for compensation of time-base error in magnetic tape recorder data. A buffer shift register with feedback control is used to obtain a variable delay of the recorded signal during playback. A breadboard version is described and typical experimental results are provided to demonstrate the performance of the system. A mathematical model of the system is developed and justified by comparing analytical results with data from the breadboard model. The feasibility of the technique for airborne tape recorders is predicted based upon an estimate of system weight, size, and cost.

ACKNOWLEDGEMENT

TABLE OF CONTENTS

LIST OF FIGURES

LIST OF SYMBOLS

$A(j\omega)$	Control-loop gain function
C	Overall recorder gain
C_b	Buffer capacity
$d_i(t)$	Instantaneous buffer input rate deviation
$d_o(t)$	Instantaneous buffer output rate deviation
$D_i(s)$	Laplace transform of $d_i(t)$
$D_o(s)$	Laplace transform of $d_o(t)$
$e_d(t)$	Discriminator output voltage
$e_i(t)$	Recorder input voltage
$e_m(t)$	Voltage modulation signal
$e_o(t)$	Recorder output voltage
E_c	Peak amplitude of sinusoidal carrier
E_m	Peak amplitude of voltage modulation signal
$f(t)$	Instantaneous frequency
f_o	Sinusoidal frequency
$g(t)$	Overall flutter
$g_r(t)$	Recording flutter
$\lvert G(\omega) \rvert$	Flutter amplitude spectral density (Hz^{-1})
$G_c(s)$	Compensator network transfer function
G_o	Uniform flutter spectral density (Hz^{-1})
$h(t)$	Overall time-base error in seconds (s)
$h_o(t)$	System output time-base error

$h_p(t)$	Playback time-base error
$h_r(t)$	Recording time-base error
$|H(\omega)|$	TBE amplitude spectral density (s/Hz)
$H_o(s)$	Laplace transform of $h_o(t)$
$H_1(s)$	Rate-deviation transfer function
$H_2(s)$	Queue-error transfer function (s)
k	Multiple of σ_q defining required buffer capacity
K	Control-loop gain (s^{-1})
K_b	Buffer gain (V/words)
K_d	FM discriminator gain-conversion constant (V/Hz)
K_p	Playback constant (V/Wb)
K_r	Recording constant (Wb/V)
K_v	VCO gain (wps/V)
M_p	Maximum magnitude of $H_1(j\omega)$
$n(t)$	Control voltage for data and pilot signal VCO's
N	Number of bits in each digital word
$P_{ou}(k)$	Probability of buffer overflow or underflow
$q(t)$	Instantaneous queue
$q_e(t)$	Queue-error
q_o	Reference queue
$q_{ss}(t)$	Steady state queue-error
$Q(s)$	Laplace transform of $q_e(t)$
$r_i(t)$	Instantaneous buffer input rate
$r_o(t)$	Instantaneous buffer output rate
R_o	Mean buffer input and output rate
s	Complex frequency variable
t	Time

$v_r(t)$	Instantaneous recording tape velocity
v_p	Mean playback tape velocity
v_r	Mean recording tape velocity
x	Distance along tape
β_c	Frequency at which $\left| A(j\omega) \right| = 1$
$\Delta f(t)$	Instantaneous frequency deviation
$\Delta\omega_c$	Peak carrier angular frequency deviation
λ	Minimum logic switching time
σ_g^2	Variance of flutter amplitude
σ_h^2	Variance of TBE
σ_q^2	Variance of queue-error
τ_i	Compensator network time constants $(i = 1,2,3)$
$\phi(x)$	Flux established on tape (Wb)
$\phi_q(\tau)$	Autocorrelation function of queue-error
$\Phi_{d_i}(\omega)$	Spectral density of input rate deviation
$\Phi_q(\omega)$	Spectral density of queue-error
Ψ	System phase margin
ω	Angular frequency
ω_a	Lower frequency limit of flutter spectral density
ω_b	Upper frequency limit of flutter spectral density
ω_c	Angular frequency of carrier
ω_m	Frequency at which M_p occurs
ω_o	Sinusoidal angular frequency

CHAPTER 1

INTRODUCTION

Magnetic tape recorders are required in space telemetry systems
for both airborne recording of data to be retransmitted at a later
time and for temporary storage of signals received at ground stations.
Distortion in the recording process contributes to the bit synchroni-
zation problem in transmitting high-rate digital data and also results
in errors during demodulation of analog signals [1] . The purpose of
this study was to develop a system which could be used to compensate
for time base distortion in digital or analog recorders in either
application.

1.1 BACKGROUND

The primary source of recorder distortion is the instantaneous
velocity variation in the magnetic tape during the record and reproduce
processes. The velocity variation, defined as flutter [2] , is the
result of various mechanical imperfections in the tape transport
mechanism, such as eccentricities in the capstan, pinch rollers, and
idlers. Other sources are friction between the granular tape coating
and transport surfaces and non-uniform tape tension. Precise servo
systems have been developed to control the position and speed of the
tape, but electro-mechanical control systems have limited bandwidths
and cannot eliminate the higher frequency components of flutter.
The results of studies on the flutter phenomenon [3, 4] show that the

major flutter effect is a time-base error (TBE) in the recorded signal.
Hence, recent design efforts have been in the direction of compensating
for TBE rather than eliminating flutter itself. Chao [5] has implemented
two systems for TBE compensation. The first of these reduces the TBE
of the distorted data signal by passing it through a variable delay line,
where the delay is controlled by the TBE of a recorded pilot signal.
The second system samples the data signal at a constant rate, stores
the sample voltages on capacitors, and then recombines the samples
after a variable delay which is again controlled by a pilot signal TBE.

1.2 ANALYSIS OF FLUTTER EFFECTS IN TAPE RECORDERS

The effects of flutter can be demonstrated by deriving the output
expressions for two common magnetic tape recording techniques [6] .

1.2.1 Direct Recording Systems

The direct recording technique utilizes a current proportional to
the data signal to drive the recording head winding. During playback
a flux change in the playback head induces a voltage proportional to
the derivative of the recorded signal in the head winding. Equal-
ization networks are then used to recover the original data signal
from the playback voltage.

The instantaneous flutter during recording, $g_r(t)$*, is defined
relative to tape velocity as

$$g_r(t) = \frac{v_r(t) - V_r}{V_r} , \qquad (1.1)$$

where V_r is the mean record tape velocity and $v_r(t)$ is the instantaneous

*All symbols used in this report are listed in the List of Symbols
on page viii.

tape velocity. The distance along the tape, x, is obtained by integrating $v_r(t)$ with respect to time. Hence,

$$x = V_r \left[t + h_r(t) \right] , \qquad (1.2)$$

where the deviation in the time base, $h_r(t)$, is defined as TBE and is related to flutter by the expression

$$h_r(t) = \int_0^t g_r(\alpha) \, d\alpha . \qquad (1.3)$$

The flux established on the tape is proportional to the data signal, $e_i(t)$ and using (1.2) can be expressed as a function of tape displacement.

$$\phi(x) = K_r \, e_i \left\{ x/V_r - h_r(x/V_r) \right\} . \qquad (1.4)$$

The voltage induced in the playback head winding, $e_o(t)$, is proportional to the time derivative of $\phi(x)$ and can be expressed as a function of the playback time by using the relationship

$$x = V_p \left[t + h_p(t) \right] , \qquad (1.5)$$

where V_p is the mean playback tape velocity, and $h_p(t)$ is the playback TBE. Thus, for V_r equal to V_p,

$$e_o(t) = K_r K_p \left[1 - \dot{h}_r \left\{ t + h_p(t) \right\} \right] \left[1 + \dot{h}_p(t) \right]$$
$$\cdot \dot{e}_i \left\{ t + h_p(t) - h_r \left\{ t + h_p(t) \right\} \right\} , \qquad (1.6)$$

where time differentation is indicated by dot ($\bullet$) e.g., $\dot{h}_p(t)$. The overall TBE is defined as

$$h(t) = h_p(t) - h_r \left\{ t + h_p(t) \right\} , \qquad (1.7)$$

and overall flutter is defined as

$$g(t) = \dot{h}(t). \qquad (1.8)$$

Using (1.7), (1.8), and defining $C = K_r K_p$, (1.6) simplifies to

$$e_o(t) = C \left[1 + g(t) \right] \dot{e}_i \left\{ t + h(t) \right\}. \tag{1.9}$$

It is apparent that tape-recorder flutter results in a perturbation of the time base and a modulation of the amplitude of the data signal. Since typical peak magnitudes of $g(t)$ vary from 5×10^{-4} to 2×10^{-3}, the output voltage expression is approximated by

$$e_o(t) = C \dot{e}_i \left\{ t + h(t) \right\}. \tag{1.10}$$

1.2.2 FM Recording Systems

The FM recording technique utilizes a current proportional to an FM modulated carrier to drive the recording head winding. The voltage induced in the head winding during playback is demodulated to recover the original data signal.

The input signal is of the form

$$e_i(t) = E_c \sin \left(\omega_c t + \frac{\Delta \omega_c}{E_m} \int_0^t e_m(\alpha) \, d\alpha \right). \tag{1.11}$$

The playback voltage is obtained by substituting (1.11) into (1.9). An expression corresponding to the demodulator output is then obtained by taking the time derivative of the argument of the resulting cosine term to give

$$e_d(t) = K_d \omega_c g(t) + K_d \Delta\omega_c \left[1 + g(t) \right] \frac{e_m \left\{ t + h(t) \right\}}{E_m}. \tag{1.12}$$

The first term in (1.12) is an additive noise signal which is normally eliminated by subtracting from the discriminator output a voltage proportional to the recorder flutter. The expression $1+g(t)$ is an amplitude modulation of the output signal, as it was in direct recording, and is commonly eliminated by controlling the discriminator gain with

a signal proportional to the flutter. Hence, if these compensation techniques are used or if the flutter magnitude itself is small, (1.12) reduces to

$$e_d(t) = K_d \; \Delta\omega_c \; \frac{e_m \{t + h(t)\}}{E_m} , \tag{1.13}$$

which illustrates that TBE is the major effect of flutter.

1.3 FLUTTER AND TBE SPECTRA

The spectral density of flutter, $|G(\omega)|^2$, can be represented with a rectangular model [7] , as shown in Fig. 1.1. The lower end of the spectrum, ω_a, is determined by the bandwidth of the recorder tape control mechanism. High performance recorders have precise feedback speed controllers to eliminate the significant flutter components below 50 or 100 Hz, leaving a uniform flutter spectrum extending to 10 kHz or more. The flutter in this region is generated by random effects such as friction between the granular coating on the tape and recorder surfaces.

These random disturbances result in a flutter amplitude which can be represented as a normally distributed random variable with zero mean and variance given by

$$\sigma_g^2 = \frac{G_o}{2\pi} (\omega_b - \omega_a), \tag{1.14}$$

where G_o is the uniform spectral density. Using (1.8), the TBE transform is

$$H(\omega) = \frac{G(\omega)}{\omega} , \tag{1.15}$$

so the TBE power density is

$$|H(\omega)|^2 = \frac{G_o}{\omega^2} , \tag{1.16}$$

$$\left| G(\omega) \right|^2$$
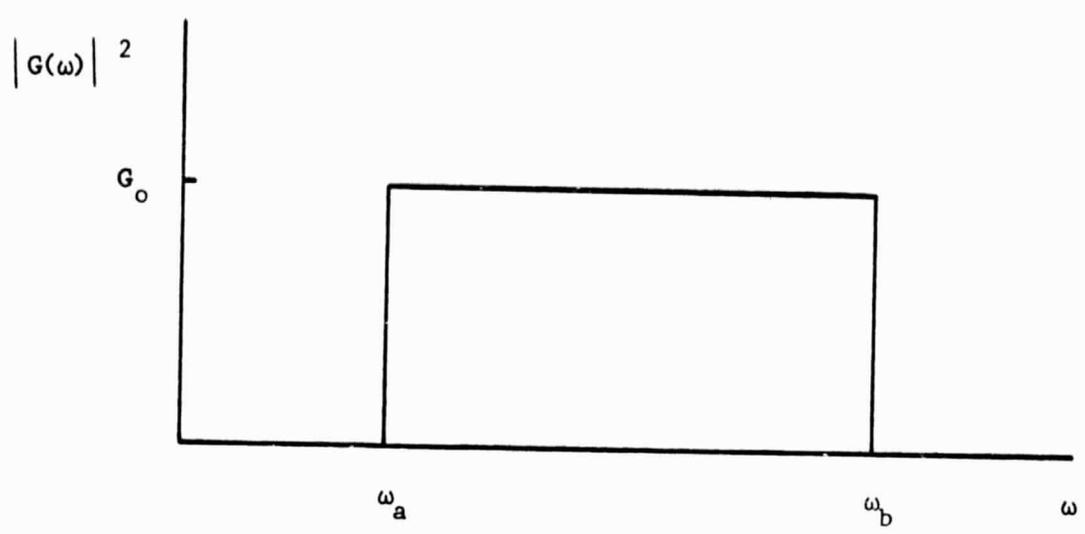
Fig. 1.1. Flutter Power Spectrum .

$$\left| H(\omega) \right|^2$$
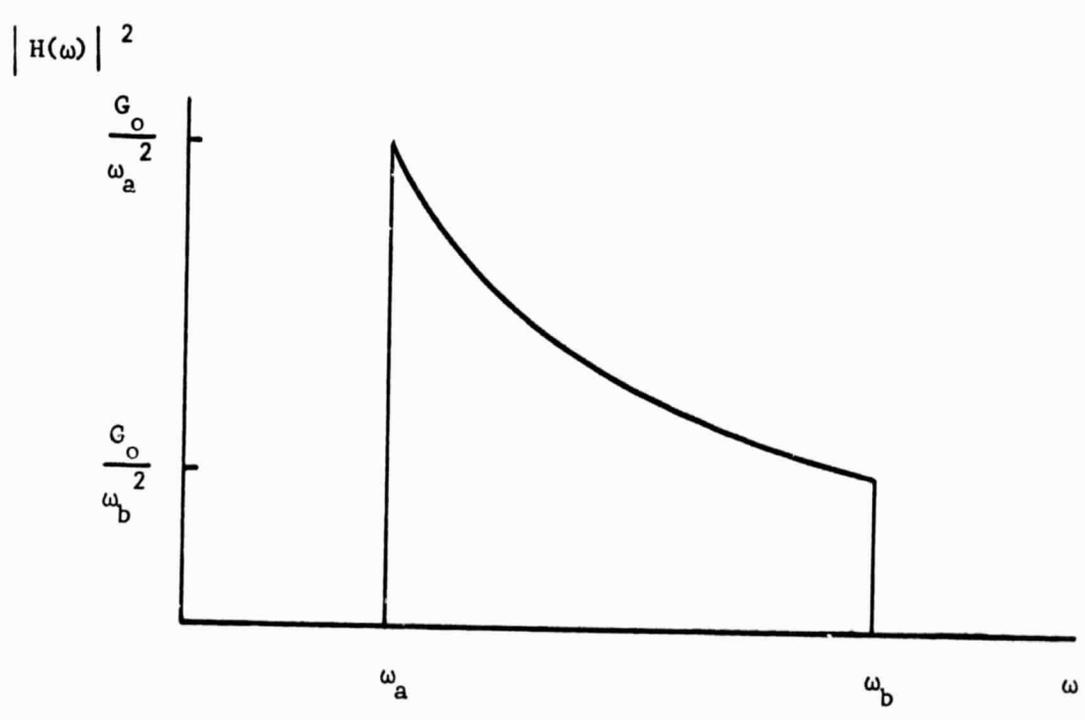
Fig. 1.2. TBE Power Spectrum .

as displayed in Fig. 1.2. The mean-square value of TBE is

$$\sigma_h^2 = \frac{1}{2\pi} \int_{\omega_a}^{\omega_b} \left| H(\omega) \right|^2 d\omega. \qquad (1.17)$$

Substituting (1.14) and (1.16) into (1.17), and integrating gives

$$\sigma_h^2 = \frac{\sigma_g^2}{\omega_a \omega_b}. \qquad (1.18)$$

The significance of low-frequency flutter is evident from (1.18) and Fig. 1.2. The magnitude of TBE may become quite large if ω_a is small. Typical peak magnitudes of TBE are 2 μs or less for the high performance recorders, but may be as high as 200 μs or more for recorders which do not have an effective speed servo [8] .

1.4 OUTLINE

A system is presented in this report for partially compensating the residual TBE found in magnetic tape recorders. The system employs a digital buffer having an output rate which is controlled such that the data is read out at a more uniform rate than it is received. The basic operation of the system and the establishment of a mathematical model for the control loop are discussed in Chapter 2. The implementation of the technique, the procedure for selecting system parameters, and a comparison of experimental and theoretical results are presented in Chapter 3. The advantages, limitations, and possible refinements of the digital technique are discussed in Chapter 4. Details of the digital logic, a design example, and measurement methods used to obtain the experimental results are included in the Appendices.

CHAPTER 2

DIGITAL TECHNIQUES FOR TBE COMPENSATION

Two digital techniques for TBE compensation are described. The first, an ideal method, would virtually eliminate TBE in the read-out data, but would require a buffer of infinite capacity. The second employs a feedback control loop to reduce the buffer capacity to a few words at the expense of not completely removing the TBE in the output data. Finally, a mathematical model of the control loop is defined and the system transfer functions derived.

2.1 INFINITE BUFFER

The TBE of a recorded signal can theoretically be eliminated by inserting a variable-time delay line in the signal path and controlling the delay with another signal corresponding to the recorder flutter. However, this approach has restricted application because of the expense, physical size, and limited delay capabilities of the line. An alternate method of obtaining a variable delay is to sample the data signal at a rate corresponding to uniform sampling in the absence of TBE and to hold the sample values for a controlled period of time before reconstruction. The use of this technique to compensate for TBE is illustrated by the waveforms shown in Fig. 2.1. The data signal and a constant frequency pilot signal are recorded on two channels of the recorder. If the tape skew effects are assumed to be negligible, both signals have the same time base perturbation on playback. Sampling the data signal during
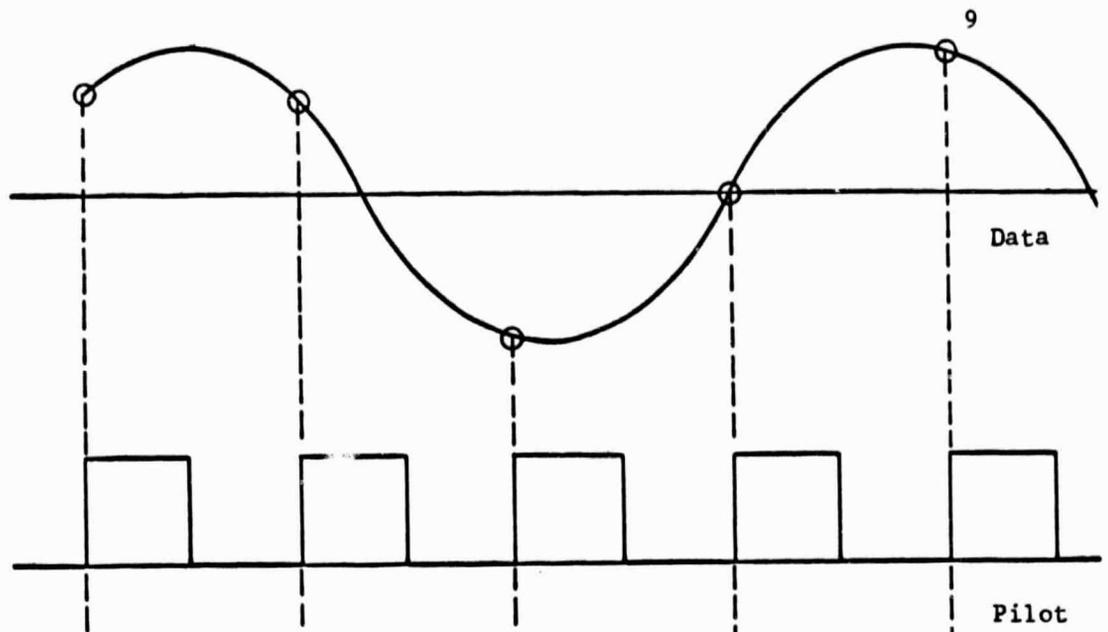
(a) Recorder Input Data and Pilot Signals
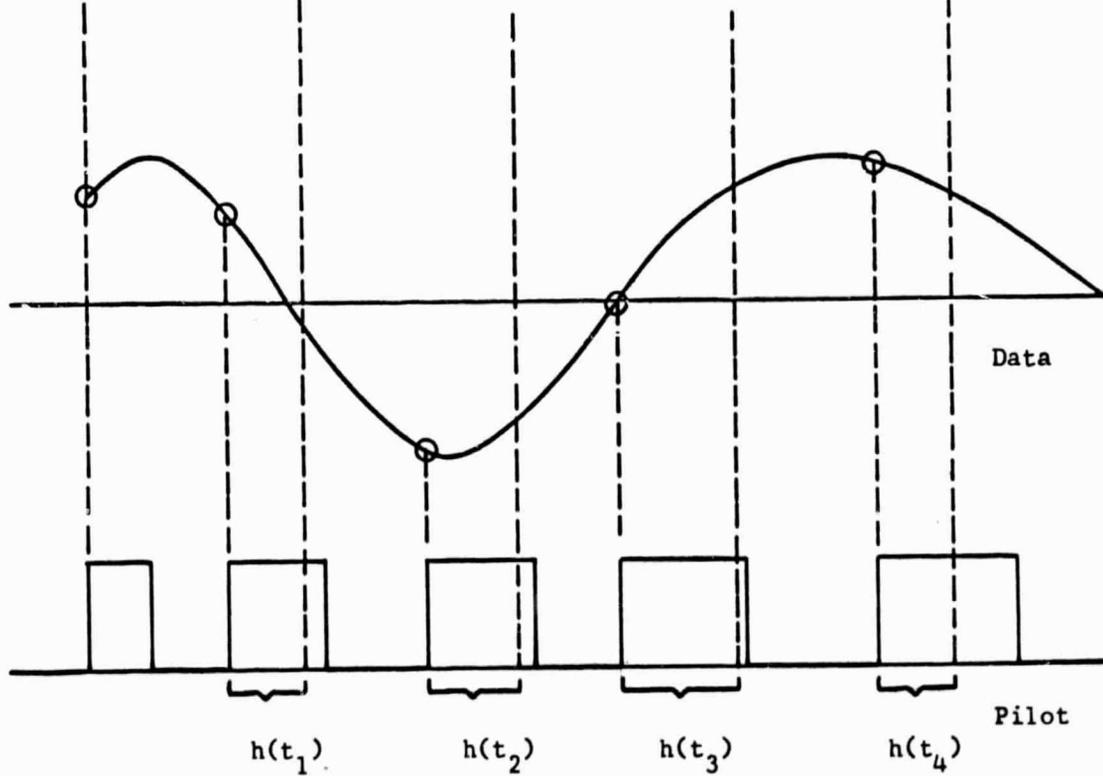
(b) Reproduced Data and Pilot Signals

Fig. 2.1. Time Relations Between Recorder Input and Output.

playback at times corresponding.to the leading edges of the pilot signal, is equivalent to uniformly sampling of the original signal in the absence of TBE. Consequently, the original data signal can be recovered completely by recombining the sample values placed in time at points corresponding to the original pilot pulses.

The block diagram of a digital system employing the sample-and-hold technique is shown in Fig. 2.2. The sample values are converted to digital words by the A/D converter and stored in a buffer shift register. The words are then gated out by the output oscillator and converted back to an analog signal with the D/A converter. The same technique can be employed with digital data, however, the need for the A/D and D/A converters is obviously eliminated.

Since the input rate depends on the flutter of the tape recorder and the output rate is constant, it is possible to have overflow or underflow of the buffer in some period of time. Buffer overflow occurs if the total number of words read into the buffer less the number read out is greater than the word storage capability of the buffer; whereas, underflow occurs if the output rate is greater than the input rate over a period of time. One way to prevent these errors is to add more stages to the buffer and reduce the output rate, but it is obvious that this solution is unrealistic since any static difference in the pilot signal and output oscillator frequencies would require an infinite buffer to prevent data loss. Even if the oscillators were synchronized perfectly, the magnitude of the recorder flutter could require an impractical buffer length.

2.2 FEEDBACK CONTROL

A buffer control loop [9] can be used to reduce the storage
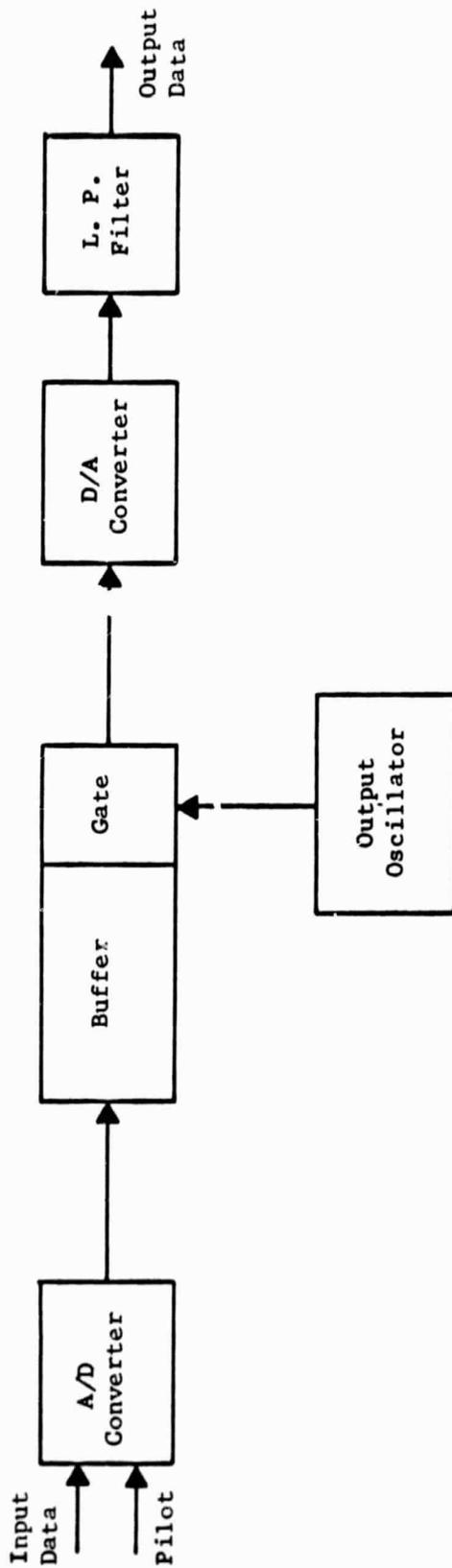
Fig. 2.2. Block Diagram of TBE Compensation System.

requirements of the digital system. Feedback control of the output
rate to prevent data loss is obtained by the technique illustrated in
Fig. 2.3. The input to the system is a series of binary digits (bits)
with an instantaneous rate, $r_i(t)$ bits/second (bps). The buffer is a
flip-flop shift register which stores the bits until they are read out
by the gate. The instantaneous output bit rate, $r_o(t)$, is equal to
the frequency of the voltage-controlled oscillator (VCO).

The VCO control voltage is derived from a measure of the total
buffer queue, $q(t)$, which is the number of bits stored in the buffer.
The difference between total queue and a reference queue, q_o, is defined
as the queue-error, $q_e(t)$.

$$q_e(t) = q(t) - q_o. \qquad (2.1)$$

The voltage from the queue-sense circuit, $K_b q_e(t)$, is applied to the
loop filter for smoothing and used to regulate the VCO frequency. The
output bit rate is determined by the VCO gain, K_v, as well as the filter
characteristics and the queue signal. As the queue-error increases or
decreases, the output bit rate increases or decreases accordingly to
prevent a tendency toward buffer overflow or underflow.

The overflow and underflow errors can be defined in terms of total
queue and buffer capacity, C_b, which equals the number of flip-flops in
the shift register. Buffer overflow occurs whenever $q(t) > C_b$; like-
wise, buffer underflow occurs whenever $q(t) < 0$. A constraint on
queue-error to prevent underflow or overflow can be expressed using
these definitions and (2.1).

$$- q_o \leq q_e(t) \leq C_b - q_o. \qquad (2.2)$$

Normally, the reference queue would be established at one-half the
buffer capacity so that both underflow and overflow would be equally
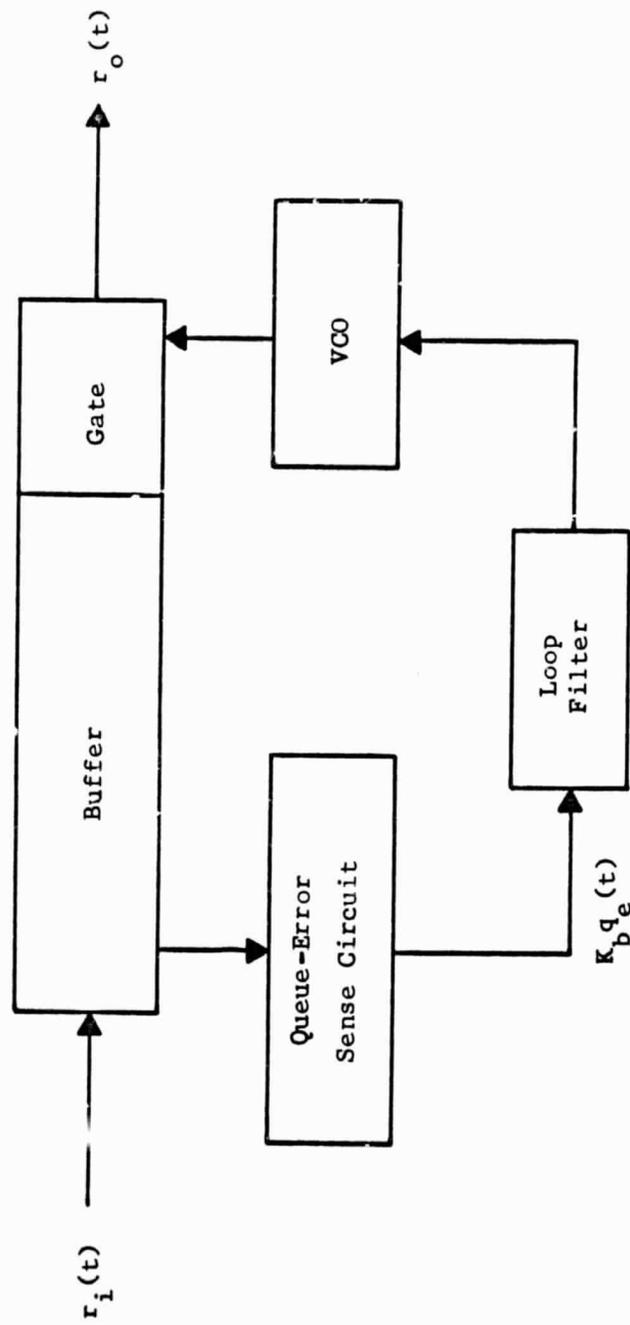
Fig. 2.3. Block Diagram of Buffer Control Loop.

improbable. Thus, the queue-error constraint becomes

$$\left| q_e(t) \right| \leq C_b/2. \tag{2.3}$$

The loop filter and gains K_b and K_v determine how fast the output bit ι.ce responds to a change in queue. These parameters are chosen so that a desired reduction in the bit-rate variation is obtained without exceeding the limits on queue expressed in (2.3).

Since the output of the A/D converter is a binary word consisting of N parallel bits, the buffer must contain N serial shift registers, each of which consists of C_b flip-flops. Thus, the buffer has the capability of storing up to C_b digital words of size N bits. A word is transferred into or out of the buffer by simultaneous application of the appropriate control pulse to all of the shift registers. Since the number of words stored in the buffer is always equal to the number of bits stored in a single shift register, the system can be regulated by one buffer control loop. Consequently, all of the capacity and rate variables associated with the buffer and its control system will be redimensioned in terms of words or words/s (wps) instead of bits or bps.

2.3 DERIVATION OF MODEL

A mathematical model of the control loop can simplify the problem of selecting system parameters. It has been observed that in order to eliminate TBE it is necessary that $r_o(t)$ should be constant. Furthermore, it was shown in Section 2.2 that a constraint on $q_e(t)$ must be satisfied to prevent loss of data during temporary storage. Hence, the desired relationships to predict system performance are expressions for $q_e(t)$ and $d_o(t)$, the instantaneous deviation of $r_o(t)$ from its mean

value R_o.

$$d_o(t) = r_o(t) - R_o. \tag{2.4}$$

Similarly, the data rate into the control loop, $r_i(t)$, has an instantaneous deviation given by

$$d_i(t) = r_i(t) - R_o. \tag{2.5}$$

Thus, the total number of words stored in the buffer at time t is given by

$$q(t) = \int_0^t r_i(\lambda)\, d\lambda - \int_0^t r_o(\lambda)\, d\lambda + q_o, \tag{2.6}$$

where q_o is the number of words stored at time zero. Combining (2.1), (2.4), (2.5), and (2.6) yields

$$q_e(t) = \int_0^t \left[d_i(\lambda) - d_o(\lambda) \right] d\lambda. \tag{2.7}$$

The transform of the queue-error, $Q(s)$, can be obtained by taking the Laplace transform of (2.7) giving

$$Q(s) = \left[D_i(s) - D_o(s) \right] / s. \tag{2.8}$$

It can be seen from inspection of Fig. 2.3 that the output voltage transform of the queue-error sense circuit is $K_b Q(s)$, and the transform output of the loop filter is $K_b G_c(s) Q(s)$, where $G_c(s)$ is the voltage-ratio transfer function of the filter. Since the VCO can be represented by a gain constant K_v, its output rate deviation transform is

$$D_o(s) = K_v K_b G_c(s) Q(s). \tag{2.9}$$

The VCO has an internal bias voltage which maintains a constant output frequency R_o. Consequently, when the input voltage is zero the output-rate deviation is zero. A mathematical model of the buffer control

loop is shown in Fig. 2.4. The rate-deviation transfer function, $H_1(s)$, and the queue-error transfer function, $H_2(s)$, can be obtained by combining (2.8) with (2.9) and defining a new constant K as the product of K_v and K_b.

$$H_1(s) = \frac{D_o(s)}{D_i(s)} = \frac{KG_c(s)}{s+KG_c(s)} \cdot \qquad (2.10)$$

$$H_2(s) = \frac{Q(s)}{D_i(s)} = \frac{1}{s+KG_c(s)} \cdot \qquad (2.11)$$

The relationship between TBE attenuation and the control-loop transfer function, $H_1(s)$, can be determined by considering the direct recording of a sinusoidal pilot signal, $\sin \omega_o t$. The output of the recorder is obtained from (1.10).

$$e_o(t) = C\omega_o \cos \omega_o \left[t + h(t) \right] . \qquad (2.12)$$

The instantaneous frequency of the pilot signal is

$$f(t) = f_o + f_o g(t), \qquad (2.13)$$

which is numerically equal to the input rate $r_i(t)$. Hence, a relationship between recorder flutter and input rate deviation can be determined by transposing f_o, or R_o, in (2.13) and comparing the result with (2.5).

$$d_i(t) = R_o g(t). \qquad (2.14)$$

Substituting (2.14) into (1.8) and integrating gives the following expression for the pilot signal TBE.

$$h(t) = \frac{1}{R_o} \int_0^t d_i(\alpha) \, d\alpha \qquad (2.15)$$

The data signal was recorded at the same time as the pilot signal; therefore, (2.15) also gives the TBE of the input data signal. Similarly,
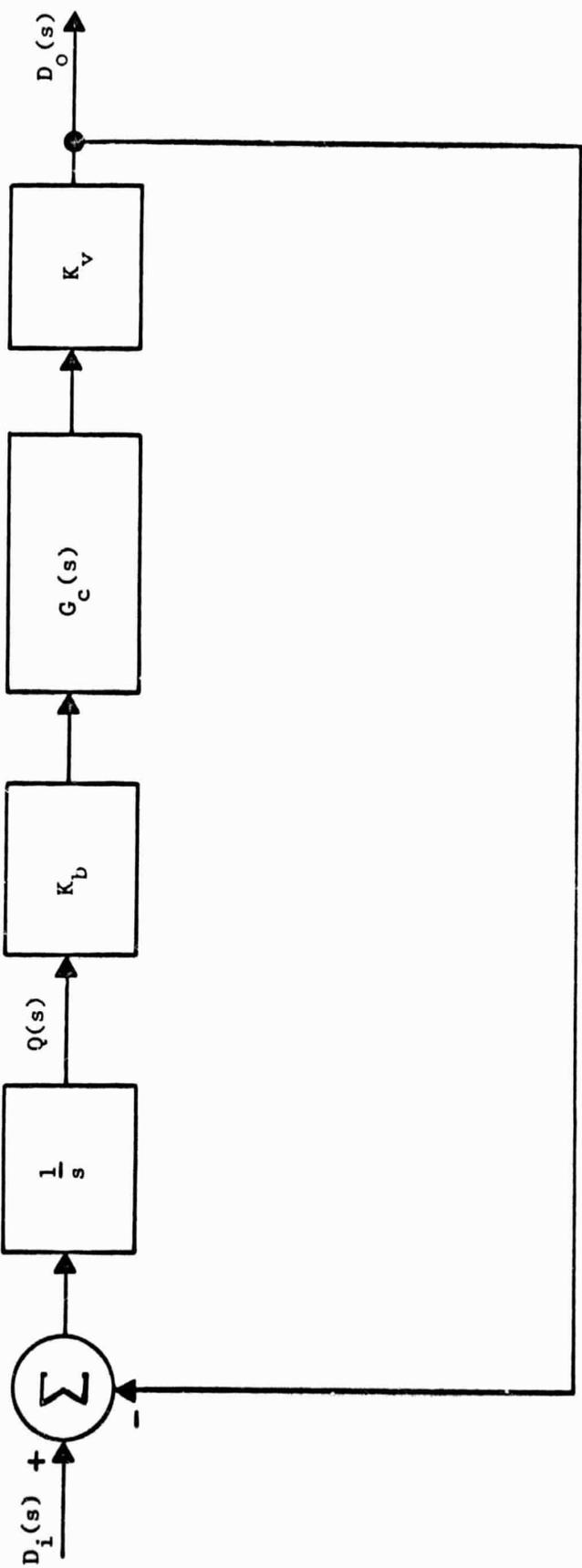
Fig. 2.4. Mathematical Model of Buffer Control Loop.

the TBE for the output data signal, $h_o(t)$, is defined as

$$h_o(t) = \frac{1}{R_o} \int_0^t d_o(\lambda)\, d\lambda \qquad (2.16)$$

Taking the ratio of the Laplace transforms of (2.15) and (2.16) yields

$$\frac{H_o(s)}{H(s)} = \frac{D_o(s)}{D_i(s)}. \qquad (2.17)$$

The relationship of (2.17) shows that the specifications of any desired TBE attenuation characteristic can be translated to requirements on the system control-loop performance.

CHAPTER 3

IMPLEMENTATION OF DIGITAL SYSTEM FOR TBE COMPENSATION

The digital circuitry used in the implementation of the system
is described briefly and results of experimental frequency responses
are presented to verify the theoretical model developed in Section
2.3. A design procedure is then outlined to indicate how given
performance specifications can be satisfied by proper selection of
values for the system parameters. Finally, the theoretical results
of a design example are verified by comparison with actual results
from the digital implementation.

3.1 DESCRIPTION OF DIGITAL SYSTEM

A block diagram of the digital system implemented in the laboratory
is shown in Fig. 3.1. (Each of the individual logic circuits is de-
scribed in detail in Appendix A.) The two inputs to the system, which
are the data signal and pilot signal, have the same amount of TBE due
to the tape recorder flutter, i.e., skew effects are presumed to be
negligible. The data signal is sampled by the A/D converter once each
pilot signal period and converted to an N-bit digital word. When
the conversion is complete, a pulse is sent to the timing logic which
then applies a read pulse to the buffer. Since the data-signal sampling
is synchronized with the positive going transition of the pilot signal,
the instantaneous rate of reading words into the buffer, $r_i(t)$, equals
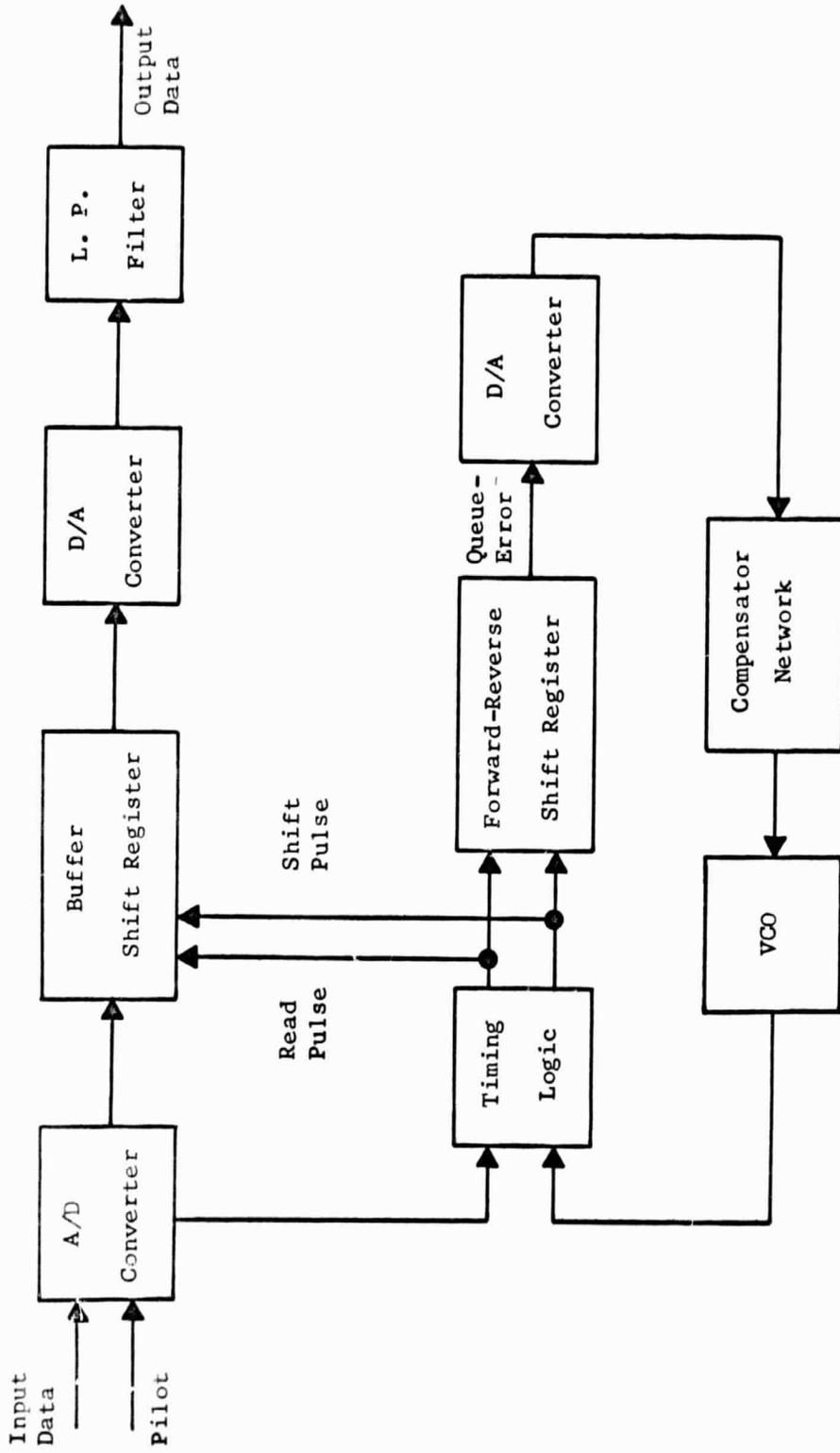the instantaneous frequency of the pilot signal.

Fig. 3.1. Implementation of TBE Compensator Using Digital Circuitry.

The words are read out of the buffer by the shift pulses from the timing logic at a rate, $r_o(t)$, equal to the instantaneous frequency of the VCO. As the words are read out of the buffer, they are converted to analog values by the N-bit D/A converter. The lowpass filter smooths the converter output to recover the data signal with TBE reduced.

The number of words stored in the buffer must be monitored to prevent overflow or underflow of the buffer. This is accomplished by using a forward-reverse shift register (FRSR) and a D/A converter to generate a signal proportional to the instantaneous queue-error. The FRSR is a series of flip-flops with the capability that a stored reference bit may be shifted in one direction for a read pulse and in the other direction for a shift pulse. Since each read or shift pulse is equivalent to a word read into or out of the buffer, the location of the reference bit is an indication of $q_e(t)$ and is converted to an analog value by the D/A converter. The queue-error voltage is then used to control the frequency of the VCO. The compensator network determines the response of the VCO frequency to a change in queue. The network attenuates the high frequency components of $q_e(t)$ to reduce the output rate variation, but passes the low frequency components to prevent data loss in the buffer.

3.2 MEASURE OF FREQUENCY RESPONSE FUNCTIONS

The mathematical model developed in Section 2.3 was verified by obtaining closed-loop frequency response functions of the laboratory system and comparing these results with the theoretical functions given by (2.10) and (2.11). The technique used to obtain the experimental data is shown in Fig. 3.2. A VCO with a center frequency of 14.3 kHz and a gain of $K_v = -40$ Hz/V was used to generate the pilot signal.
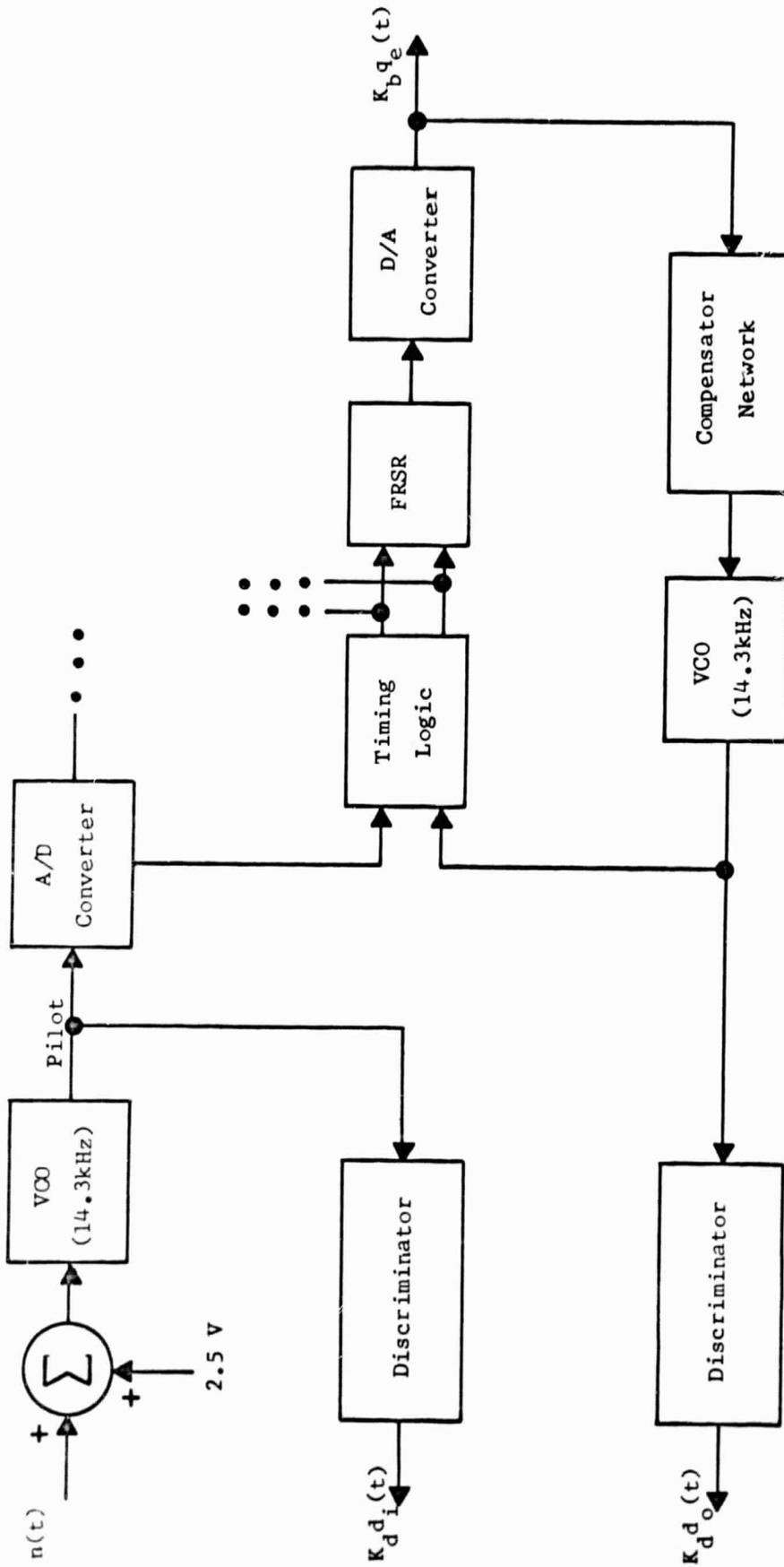
Fig. 3.2. Frequency-Response Measurement Technique.

The choice of center frequency was limited by the 100 kHz pulse repetition rate of the digital logic used. (Details of the limitation are presented in Appendix A and the implications are discussed in Chapter 4.) The input to the VCO is a voltage, $n(t)$, plus a bias of 2.5 V. Hence, the VCO output frequency is

$$f(t) = K_v \left[2.5 + n(t) \right] , \qquad (3.1)$$

where the constant term represents the VCO center frequency, f_o, and the variable term represents the instantaneous frequency deviation, $\Delta f(t)$. The frequency deviation can be related to the deviation in data rate by comparing (3.1) with (2.13) and (2.14).

$$\Delta f(t) = d_i(t). \qquad (3.2)$$

Thus, applying the pilot signal to a discriminator input yields a voltage proportional to $d_i(t)$. By similar reasoning the voltage from a discriminator monitoring the control-loop VCO is proportional to $d_o(t)$.

The frequency response functions were obtained by driving the pilot signal VCO with a sinusoidal oscillator. The maximum frequency of the oscillator was limited by the bandwidth of the discriminator. (This problem is discussed in Appendix B.) The ratio of the magnitude of $d_o(t)$ to $d_i(t)$ was obtained as a function of the oscillator frequency and is plotted in Fig. 3.3 for three values of loop gain and a unity compensator network. The theoretical curves were obtained from (2.10) with $G_c(s) = 1$.

The output of the D/A converter is a quantized voltage proportional to the queue-error, $q_e(t)$. The ratio of the magnitude of $q_e(t)$ to $d_i(t)$ was obtained as a function of the oscillator frequency and is plotted in Fig. 3.4. The theoretical curves were obtained from (2.11) with
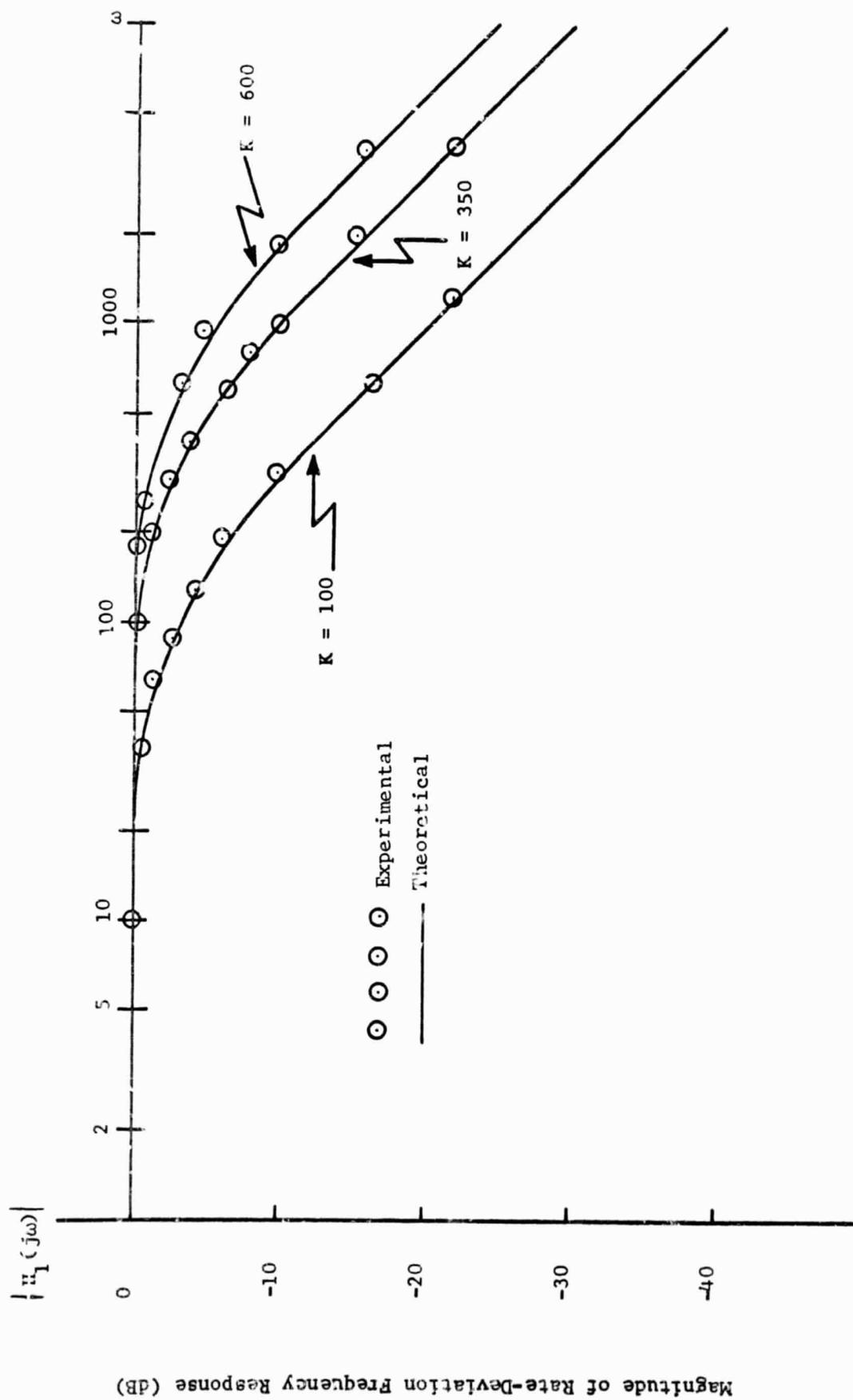
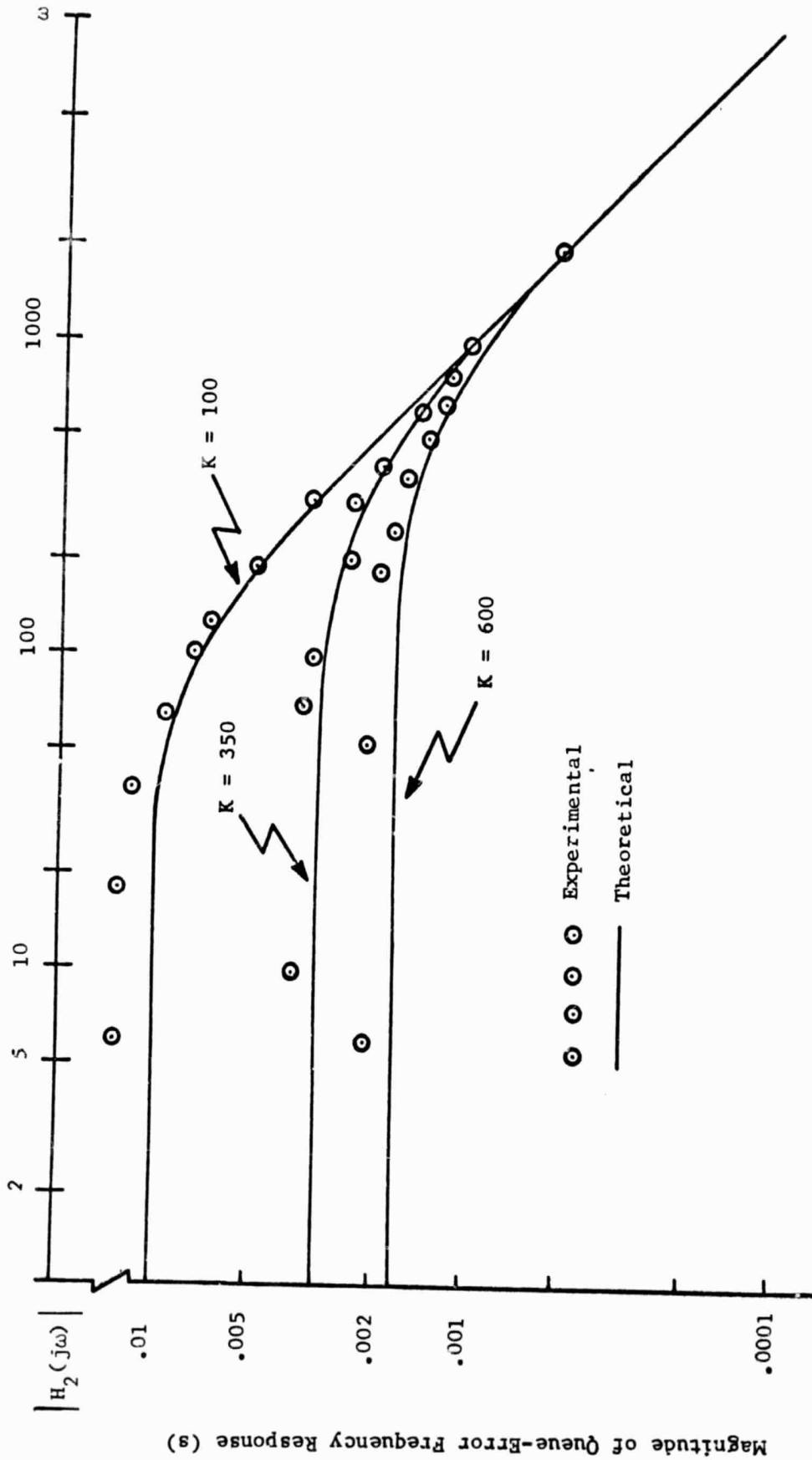Fig. 3.3. Comparison of Theoretical and Experimental Rate-Deviation Frequency Responses for Uncompensated System.

Fig. 3.4. Comparison of Theoretical and Experimental Queue-Error Frequency Responses for Uncompensated System.

$G_c(s) = 1$. The disagreement between the theoretical curves and experi-
mental values is attributed to the discrete levels in the magnitude of
the voltage $K_b q_e(t)$ and the inability to determine accurately the value
for queue-error. The discrepancy is not serious since there is close
agreement for the higher frequencies, where the more significant com-
ponents of the frequency spectrum of $d_i(t)$ will normally be found.

3.3 DESIGN PROCEDURE

The ability to derive a realistic mathematical model for the control
loop reduces the problem of selecting the system parameters to one which
can be handled by classical control system design. A design example is
presented in Appendix C to illustrate the procedure for parameter selec-
tion. The general procedure consists of the following steps.

1. Flutter Power Spectrum - The flutter power spectrum of the
tape recorder to be used is measured to determine the bandwidth and
rms value of the flutter. Measurement techniques such as cumulative
flutter graphs [10] and spectrum analysis of the frequency deviation
of a recorded sinusoid can be employed.

2. TBE Attenuation Characteristic - An approximate TBE power
spectrum is obtained from the measured flutter spectrum and is used
to determine a desired TBE attenuation characteristic, which is trans-
lated into requirements on the system closed-loop frequency response,
$H_1(j\omega)$.

3. Compensator Network and Loop Gain - A frequency domain design
technique, such as the Bode diagram, is used to determine a compensator
network and loop gain which will provide a system with the desired
closed-loop frequency response.

4. Pilot Signal Frequency - The data signals to be recorded are

analyzed to determine the highest significant frequency in the spectra. A multiple of that frequency is chosen as the pilot signal and control loop VCO center frequency.

5. <u>Queue-Error Variance</u> - The queue-error variance, σ_q^2, is determined from expressions tabulated in Appendix D, which define σ_q^2 in terms of the flutter spectral density, loop gain, compensator network transfer function, and pilot signal frequency.

6. <u>Buffer Capacity</u> - The required buffer capacity is based upon an acceptable probability of buffer overflow or underflow and is equal to a multiple of σ_q. An expression which gives the multiplier of σ_q as a function of the desired probability is derived in Appendix E.

In addition to the control loop design, a lowpass filter must be designed to smooth the output of the data signal from the D/A converter and the number of bits per digital word must be specified. The number of bits/word and the filter transfer characteristics are determined from the acceptable level of quantization error which the user can tolerate. This error is decreased as the number of bits/word is increased and as the filter characteristics approach those of an ideal lowpass filter.

3.4   EXPERIMENTAL RESULTS

The experimental performance of the system is measured in both the time and frequency domains for a system meeting the performance specifications given in Appendix C. Thus, a comparison can be made between specified and actual performance.

3.4.1   Frequency Domain

The performance of the system in the frequency domain was verified by obtaining the closed-loop frequency responses as shown in Figs. 3.5
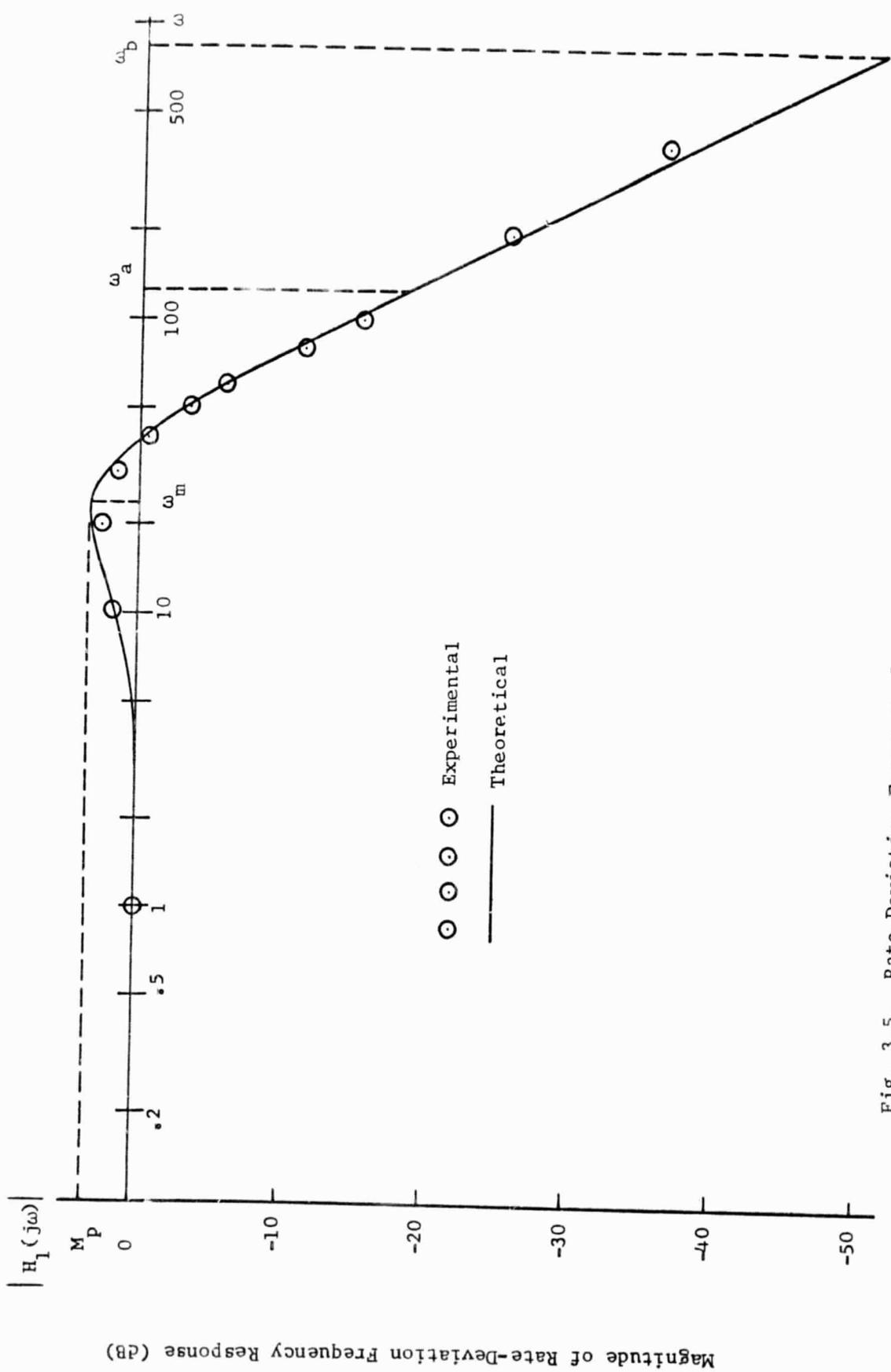
Fig. 3.5. Rate-Deviation Frequency Response for Experimental System with Compensator Network and K = 350.

28

and 3.6. The theoretical responses were determined from (2.10) and (2.11) with a loop gain of 350 and the compensator network transfer function given by (C.23). These parameters were selected in Appendix C so that $\left| H_1(j\omega) \right|$ would have a minimum of 18 dB attenuation for $\omega_a < \omega < \omega_b$, a high frequency attenuation of 12 dB/octave, and a peak value less than 1.6 (4.07 dB) which would occur at a frequency less than $\omega = 31.25$ rad/s. Inspection of Fig. 3.5 indicates that the system meets all the aforementioned specifications. The compensator network effect can be seen by comparing the response plotted in Fig. 3.5 with those of Fig. 3.3. The uncompensated system has a negligible attenuation for the frequency range of the flutter, whereas the compensated system has the desired attenuation. A slight amplification results for certain frequencies, but those frequencies are lower than the flutter spectrum. The peak value of $\left| H_2(j\omega) \right|$ also occurs at a lower frequency than the flutter spectrum, so it doesn't result in large queue-errors. The low-frequency attenuation of the response prevents any static queue-error accumulation for drifts in the pilot signal or control-loop VCO frequency. This attenuation results from the integrating effect of the compensator network. The network amplifies any low-frequency queue-error signals so that the VCO frequency is corrected and the queue-error is reduced to zero.

The spectrum of the data signal was obtained using a spectrum analyzer as shown in Fig. 3.7. The tape recorder employed in the design example was simulated with two VCO's. The spectrum of the voltage, n(t), was shaped so that the data and pilot signals appeared to be recorded sinusoids being played back by the tape recorder. (Details of the simulation are in Appendix F.) The spectra of the system input and
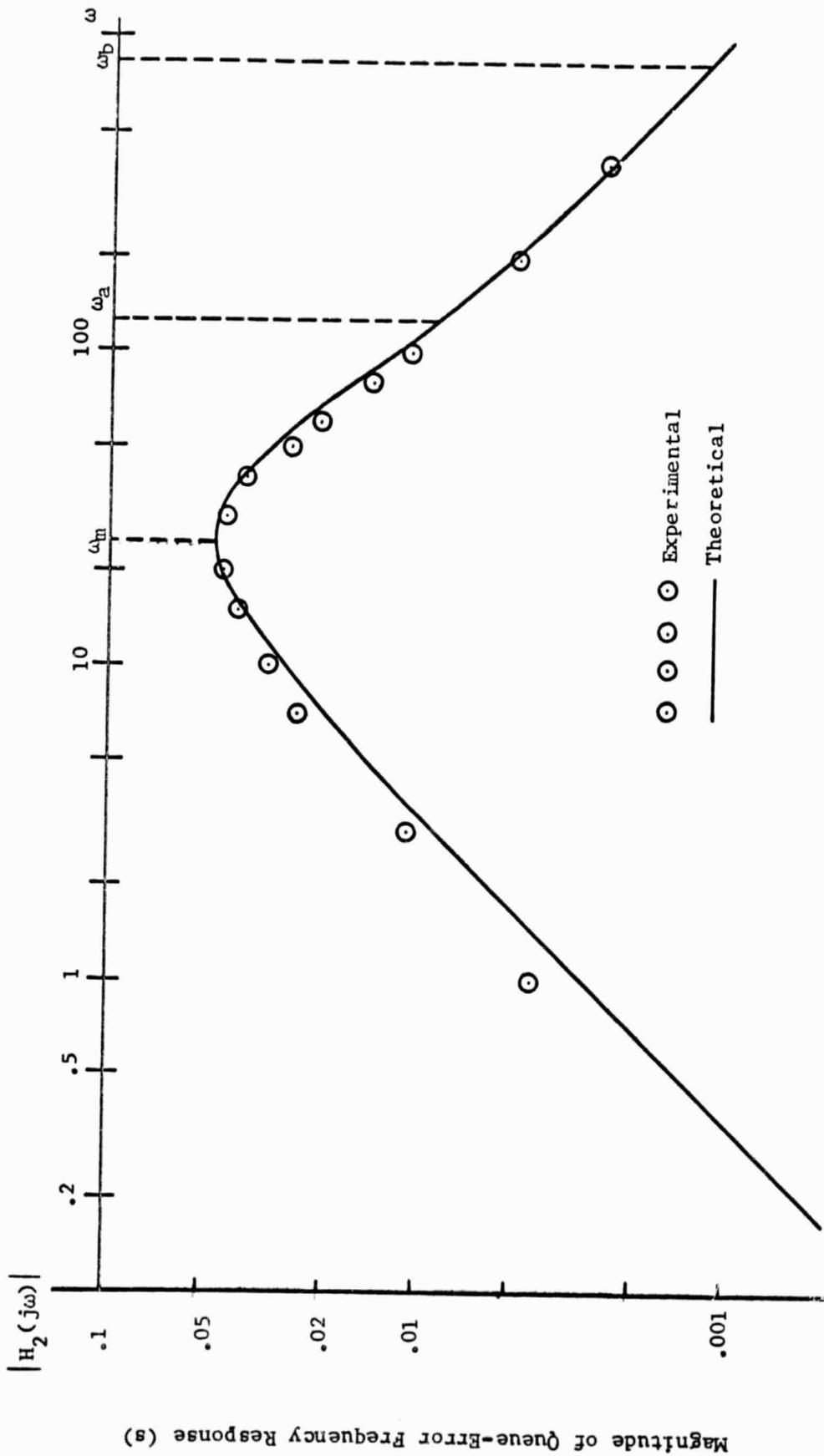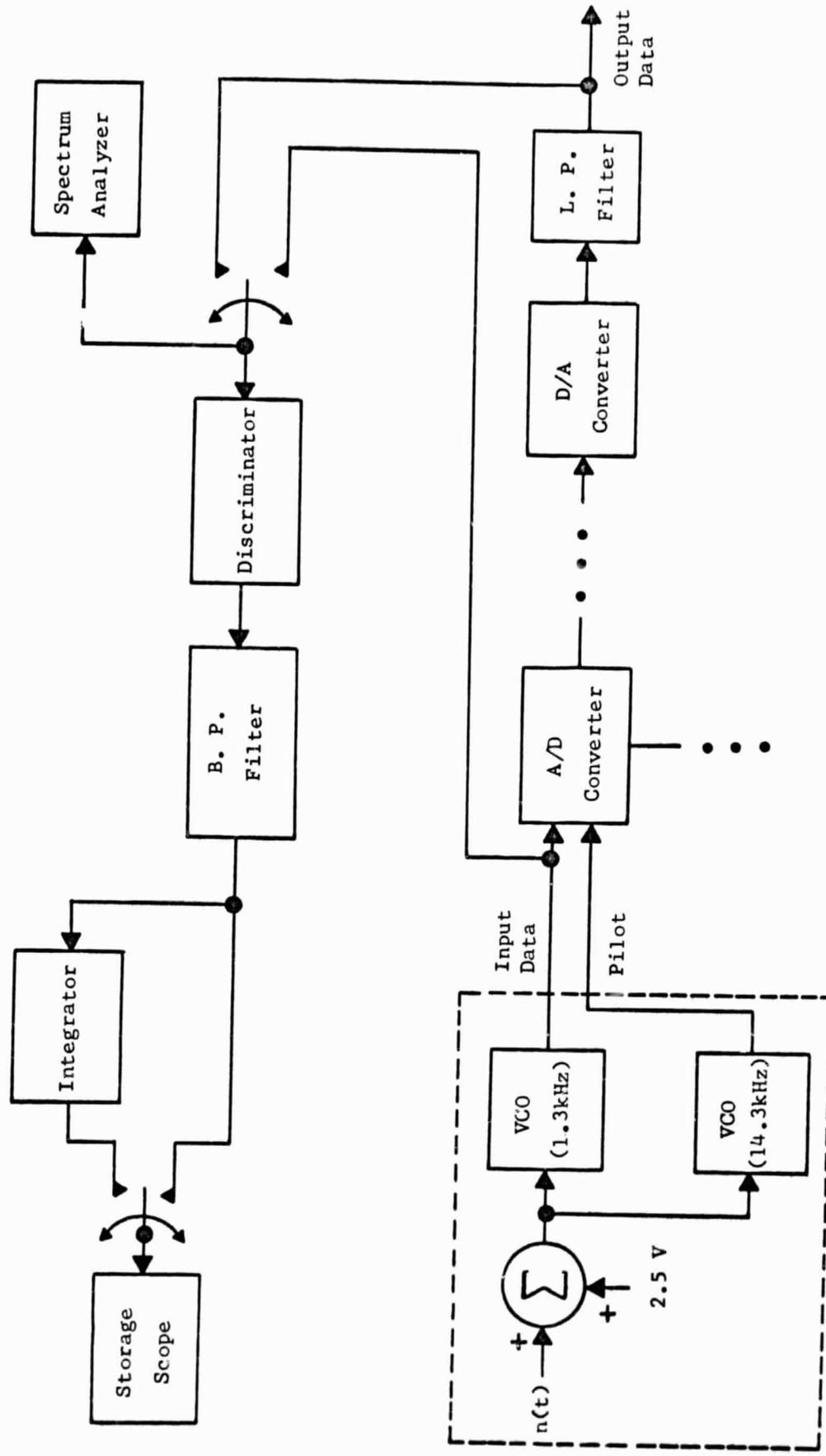
Fig. 3.6. Queue-Error Frequency Response for Experimental System with Compensator Network and K = 350.

Fig. 3.7. Data Signal Measurement Technique.

output are presented in Fig. 3.8. The spectrum of the input data signal contains frequency distortion due to the recorder flutter. A comparison of the output signal spectrum with that of a sinusoid showed the system had reduced flutter effects to a level below the resolution of the analyzer.

3.4.2 Time Domain

The time domain performance of the system was obtained with the alternate technique shown in Fig. 3.7. The instantaneous frequency deviation of the input and output data signals were measured with the discriminator and recorded with a storage scope. The bandpass filter was used to attenuate the dc offset and drift of the discriminator output and to reduce the high-frequency ripple which was not averaged by the discriminator lowpass filter. A comparison of the input and output frequency deviation is shown in Fig. 3.9. It is apparent that the output deviation is negligible. Also shown are the TBE measurements of the input and output data signals, which were obtained by integrating the instantaneous frequency deviation. The system was designed to reduce all components of TBE by at least a factor of eight or equivalently -18 dB. The peak-to-peak values of the TBE traces show that the system actually reduced TBE by more than a factor of 10.

The system was designed for a recorder flutter spectrum with a lower limit of $\omega_a = 125$. The effect of lower frequency flutter was illustrated by decreasing the lower limit to $\omega_a = 10$. Time responses obtained for the data-signal frequency deviation and TBE are presented in Fig. 3.10. The inclusion of flutter below the lower limit specified in the system design results in a doubling of the output frequency deviation and an increase of more than 15 in the peak-to-peak TBE

33
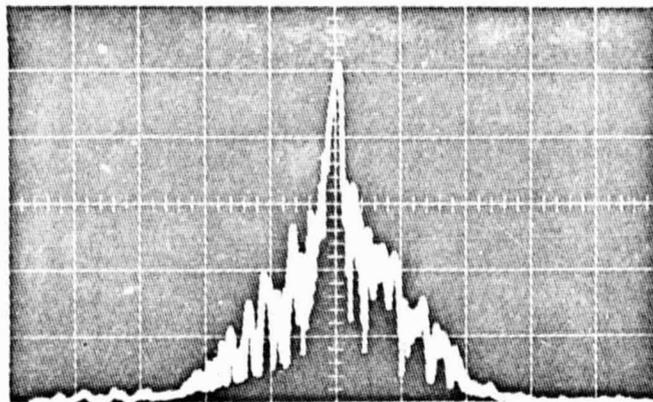
Center Frequency: 1.3 kHz
Horizontal: 100 Hz/cm

(a) Input Spectrum
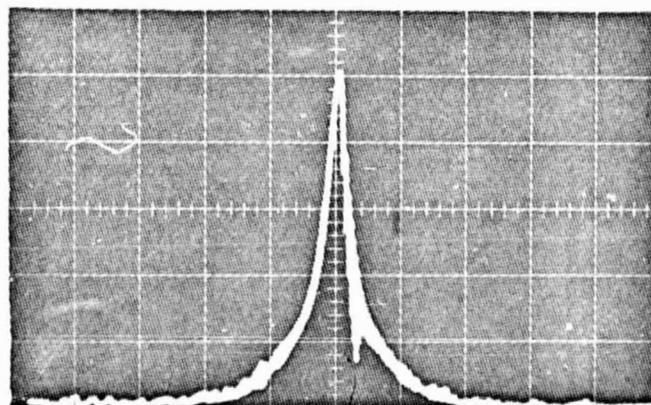
Center Frequency: 1.3 kHz
Horizontal: 100 Hz/cm

(b) Output Spectrum

Fig. 3.8. Data Signal Spectra.
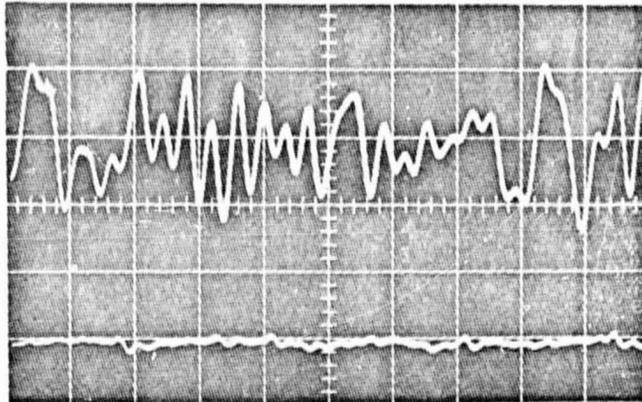
Vertical: .85%/cm
Horizontal: 20 ms/cm

(a) Instantaneous Frequency Deviation of System
      Input and Output
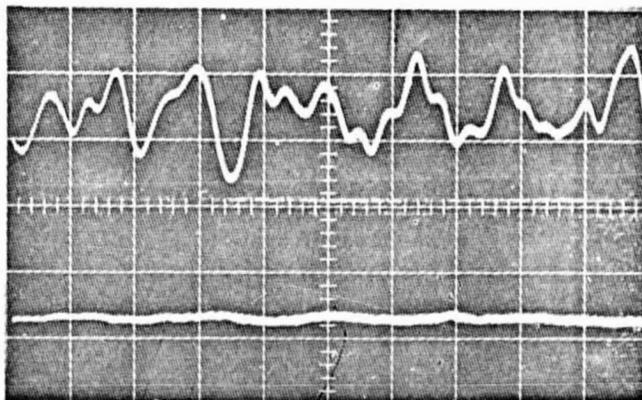
Vertical: 25 μs
Horizontal: 20 ms/cm

(b) Instantaneous TBE of System Input and Output

Fig. 3.9. Comparison of Data Signal Time Responses, $\omega_a = 125$.
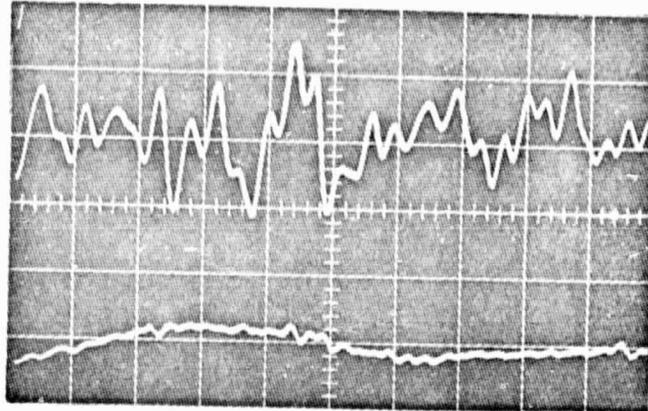
Vertical: .85%/cm
Horizontal: 20 ms/cm

(a) Instantaneous Frequency Deviation of System
     Input and Output
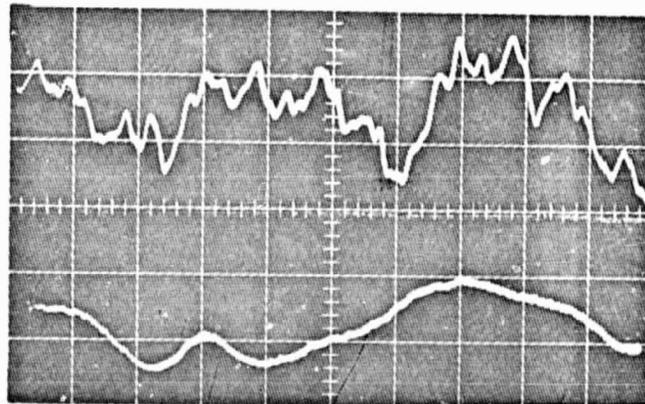
Vertical: 50 μs/cm
Horizontal: 50 ms/cm

(b) Instantaneous TBE of System Input and Output

Fig. 3.10 Comparison of Data Signal Time Responses, $\omega_a = 10$.

when compared with the results shown in Fig. 3.9. Consequently, the system control-loop must be designed for the flutter spectrum of the particular tape recorder for which compensation is required.

CHAPTER 4

APPLICATIONS OF DIGITAL SYSTEM

The advantages and limitations of the digital technique for both analog and digital recorder applications are discussed. An estimate of cost, size, and weight is provided to show the feasibility of the system for airborne applications. A possible refinement of the digital technique for use with analog recorders is also described.

4.1 ADVANTAGES AND LIMITATIONS

The fundamental advantage of the digital technique for TBE compensation is the flexibility achieved by using a feedback control loop. The performance of the system can be optimized for any application by the simple adjustment of the loop gain and compensator network components. For instance, the experimental results of Chapter 3 were obtained for a system with a two-pole compensator network, designed so that TBE would be attenuated by a minimum of 18 dB. Assuming that this attenuation was insufficient for some other application, the slope of $\left| H_1(j\omega) \right|$ could be increased to - 18 dB/octave and the TBE attenuation increased to more than 50 dB by using a four-pole compensator network. Furthermore, an integrator type compensator network can be employed in the control loop to prevent steady-state queue accumulation. The compensation methods [11] which use the pilot signal TBE to control directly the delay of the data signal cannot prevent queue accumulation since these methods do not have feedback control. Another advantage of the digital technique

is the possibility of using integrated circuits to obtain a lightweight compact system. The digital control system also has applications other than compensation of TBE in recorder data. An experimental system $\left[12\right]$ which employs the buffer control loop concept has been used to reduce the TBE of digital data transmitted over telephone channels.

The two principle limitations of the digital system are the switching speed of the digital logic and the maximum conversion rate of the A/D converter. It is shown in Appendix A that the pilot signal frequency is limited to $1/3\lambda$, where $1/\lambda$ is the maximum pulse repetition rate which can be handled by the digital logic. Current integrated circuit (IC) modules $\left[13\right]$ have operating frequencies of 6 to 10 MHz, thus limiting the pilot signal to 2 or 3 MHz. The pilot signal frequency would normally be equal to the average digital data transfer rate, $R_{()}$; thus restricting the digital compensation technique to applications where the bit rate of the recorded signal is 2 MHz or less. The conversion time of the A/D converter, approximately 1 μs for better units $\left[14\right]$, is the limiting parameter for analog recorder applications. Since the data signal is to be sampled once for each cycle of the pilot signal, the pilot signal frequency is limited to approximately 1 MHz. Consequently, if the sampling rate is 10 times the highest significant frequency of the data signal spectrum, the data signal must be band-limited to 100 kHz.

4.2 AIRBORNE RECORDERS

One of the primary applications of airborne recorders is to store digital data for retransmission at a later time. These recorders must be lightweight, compact, and reasonably inexpensive. Hence, the tape speed normally is not controlled with an electro-mechanical servo, and

the resulting increase in TBE in the transmitted digital data aggravates the problem of determining the bit timing and synchronization at the ground station.

The digital compensation system of this report is feasible for reduction of TBE in airborne recorder data. The number and type of IC's required for a system with a five stage buffer are tabulated in Appendix A. The system can be mounted on two printed circuit cards by assembling the IC modules in interconnected layers. It is estimated that an encapsulated version of the assembly would occupy less than 19 in^3. The weight of the system, not including the filling material, would be approximately 8 ozs and the components for the complete system would cost approximately $500.

4.3 PROPOSED CAPACITOR STORAGE SYSTEM

It has been noted that the TBE compensation potential of the digital system is limited by the A/D conversion time. An alternate storage technique, which eliminates the need for the A/D converter, is illustrated in Fig. 4 1. The data signal is again sampled at times corresponding to the positive going transitions of the pilot signal. However, the sample voltages are now stored on capacitors before being recombined at a rate regulated by the control loop. The location of a reference bit in each ring counter determines which capacitor is to be charged by the sample voltage and from which capacitor the output voltage is to be read. The reference bit is advanced one location in the appropriate counter for each input r output pulse. The buffer capacity of the system is equal to the number of capacitors. The queue is equal to the number of stored sample voltages and ideally is maintained at one-half of the buffer capacity, so that the read-in and read-out locations
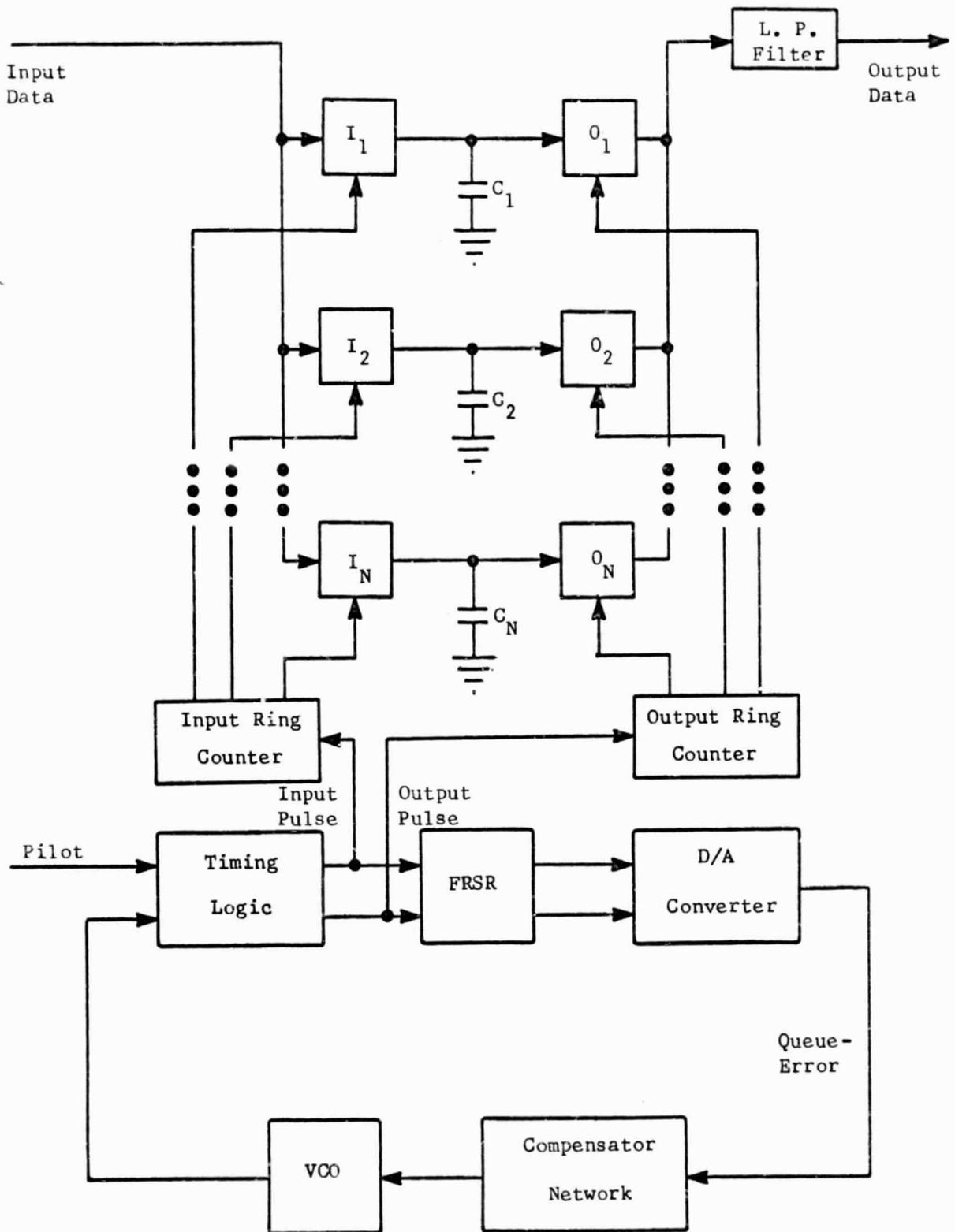
Fig. 4.1. Proposed Capacitor Storage System.

do not overlap. As in the digital storage system, the FRSR monitors
the queue-error to control the VCO frequency and thus reduce the
possibility of data loss. This technique would both increase the
acceptable bandwidth of the data signal spectrum, provided the time
required to charge the capacitors is less than 1 μs, and eliminate
the expense and complexity of high-speed A/D converters.

CHAPTER 5

SUMMARY AND CONCLUSIONS

The technique described in this report has been developed to
compensate for TBE in magnetic tape recorder data. A buffer shift
register was used to obtain a variable delay of the recorded signal
during playback. It was concluded that a buffer feedback control loop
was required to reduce the buffer capacity to a reasonable size and to
prevent data loss due to buffer overflow or underflow.

The technique was verified both with theoretical and experimental
results. An expression was derived relating the buffer input and
output rate deviation. It was shown that the system reduction of
TBE is identical to the reduction of the output data rate deviation
by the control loop. An expression derived for the relationship
between buffer queue-error and input data rate deviation confirmed
that the control-loop can be employed to reduce the required buffer
capacity.

Experimental results were obtained by implementing the system in
the laboratory with digital circuitry. Comparison of the experimental
control-loop transfer functions with the theoretical functions in-
dicated that the mathematical model was realistic. The method for
selecting system parameters was expressed as a classical control
system design problem. A design procedure was outlined, an example
was presented to illustrate the procedure, and the results of the

example were verified with the experimental system. It was shown that a minimum of 18 dB attenuation of all TBE frequency components was obtainable with a high frequency attenuation of 12 dB/octave. Additional TBE attenuation can be obtained by employing a more complex compensator network.

The compensation technique has applications for digital or analog recorders. The TBE of either digital data with bit rates up to 2 MHz or analog signals with frequency components to 100 kHz can be attenuated. A system with capacitor storage was proposed which could extend the frequency range for analog recorders. The estimates of low cost, light weight and small volume indicate that the digital technique is feasible for TBE compensation in airborne digital tape recorders.

APPENDIX A

DIGITAL LOGIC DETAILS

The digital system implemented for this study was described in Chapter 3. The details of the buffer shift register (BSR), forward-reverse shift register (FRSR), queue-error sense circuit, and timing logic are presented in this appendix. Negative logic is employed in the operation of all digital circuits described in this appendix.

A.1 BUFFER SHIFT REGISTER

The logic of a five-stage BSR is illustrated in Fig. A.1. Only one of the N serial shift registers is shown, since all of the registers are identical. Each of the registers consists of five JK flip-flops, which are clocked so that their states can change only when a positive going pulse is applied to the trigger inputs T or T_p. The contents of all registers can be reset to ZERO by applying a pulse to a common reset input.

A digital word from the A/D converter is stored in the buffer by reading one bit of the word into each register through an AND gate on the parallel set input, S_p, of one of the flip-flops. The selection of the flip-flop for bit storage is determined by the state of the Q-lines from the FRSR. The Q-line with a subscript equal to the number of words stored in the buffer will be a logic ONE and the other three lines will be at logic ZERO. Hence, only one AND gate will be enabled for each register and that gate corresponds to the flip-flop which the bit will be stored in. For instance, if two words are in the buffer,
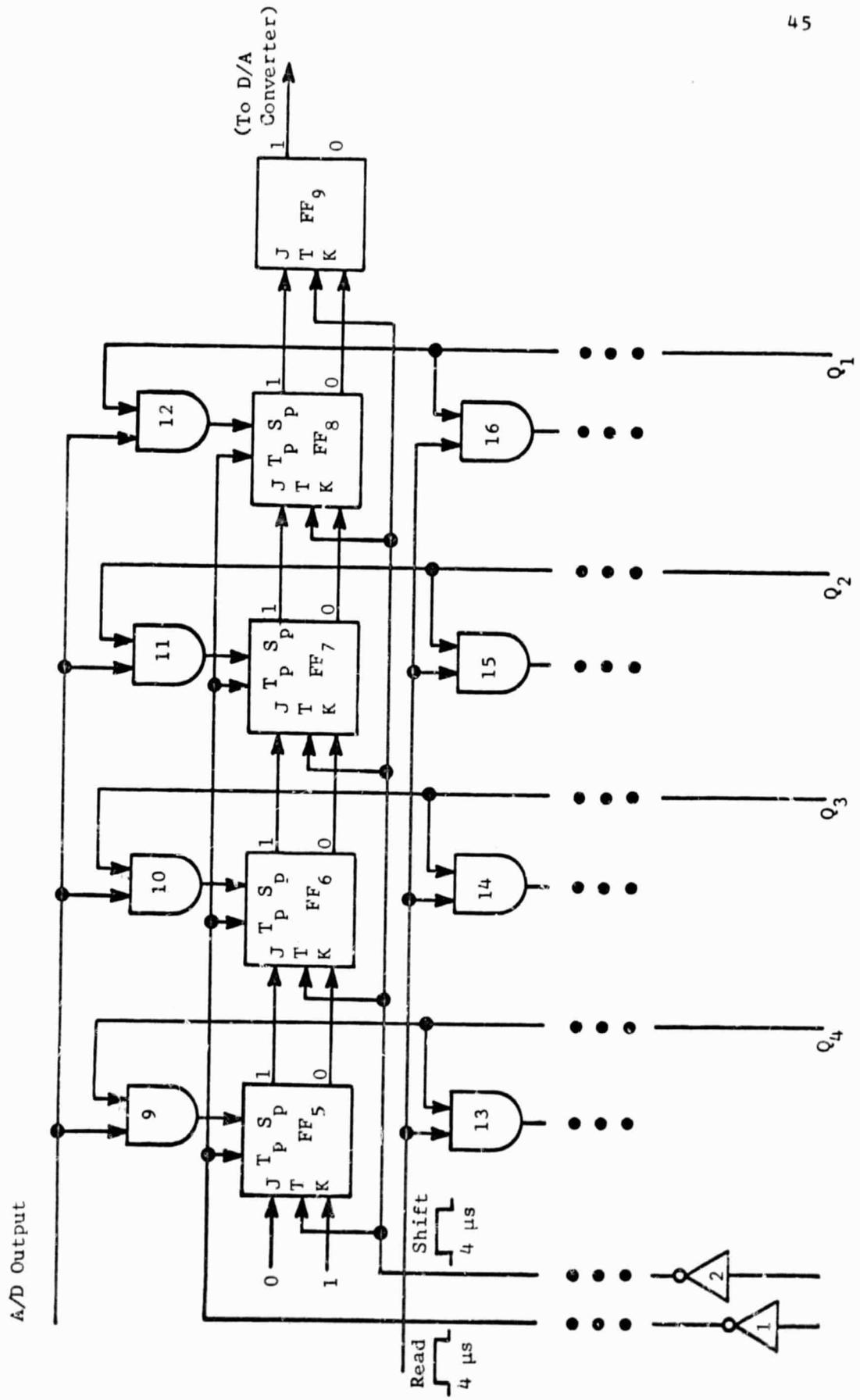
45

A/D Output

(To D/A Converter)

Fig. A.1. Buffer Shift Register Logic.

information bits will be stored in FF_8 and FF_9. Furthermore, FF_5 through FF_7 will be in the ZERO state due to an initial reset pulse, and Q_2 will be at a ONE level. If the data bit from the A/D output is a ONE, the parallel set input of FF_7 is enabled, and the read pulse sets that flip-flop to the ONE state, regardless of the logic levels on the J and K inputs. The other flip-flops are not affected, since the outputs of their AND gates are all ZERO. Conversely, if the A/D output is a ZERO, all of the S_p inputs will be at the ZERO level and FF_7 remains in the desired ZERO state after the read pulse. Either way, the register contains bits of information from three data samples. The FRSR transfers the ONE output from Q_2 to Q_3, thus insuring that the next bit will be stored in FF_6.

After each shift pulse the bits stored in the registers are transferred one place to the right and the leftmost flip-flop in each register is reset to the ZERO state. Considering the previous example, upon initiation of a shift pulse the bit stored in FF_7 will be shifted to FF_8, a ZERO from FF_6 will be shifted to FF_7, and the FRSR will change Q_2 back to a ONE so that the next bit again will be stored in FF_7. Ideally, the FRSR alternates the reference bit between Q_2 and Q_3 so that the buffer remains half full on the average; however, if the read and shift pulse rates differ due to the recorder flutter, the ONE may be transferred to Q_1 or Q_4.

The output of the rightmost flip-flop of each register represents one bit of a digital word which is converted to an analog value by the D/A converter. When the system is used to compensate TBE in a digital tape recorder, one serial shift register is required for each track.

One input to each set of AND gates would come from one recorder track, and the system output would be the output of the rightmost set of flip-flops.

A.2   FORWARD-REVERSE SHIFT REGISTER

The logic of the FRSR is shown in Fig. A.2. Initially, a RESET pulse is applied to NOR_1, OR_1, and OR_4 in order to SET FF_1 to the ONE state and RESET the other flip-flops to the ZERO state. During the RESET mode, the READ and SHIFT pulse lines are at the ZERO level to insure that the J inputs of FF_2 through FF_4 and the K input of FF_1 are ZERO. The RESET lines have no effect on the FRSR during normal operation since they will be at the ZERO level.

The stored reference bit is shifted one place to the left for each READ pulse and one place to the right for each SHIFT pulse. For example, consider the application of a READ pulse to the register when the reference bit is stored in FF_1. The output of AND_5 will be a ONE and the remaining AND gate outputs will each be ZERO. Consequently, FF_2 is the only flip-flop with a J input of ONE and is SET by the application of a TRIGGER pulse to the T input which also causes FF_1 to be RESET. Hence, the reference bit has been shifted one place to the left by the READ pulse. The operation for a SHIFT pulse is analogous.

The flip-flop TRIGGER pulse is generated by a one-shot multivibrator, OS_8, which is itself triggered by a positive-going pulse from NOR_1 corresponding to the leading edge of the READ or SHIFT pulse. The ONE output of the one-shot is used to obtain a 2 μs delay between the application of the READ or SHIFT pulse and the triggering of the appropriate

1.0
4.5
5.0
5.6
6.3
7.1
8.0
2.8
3.2
3.6
4.0
2.5
2.2
2.0
1.1
1.8
1.25
1.4
1.6
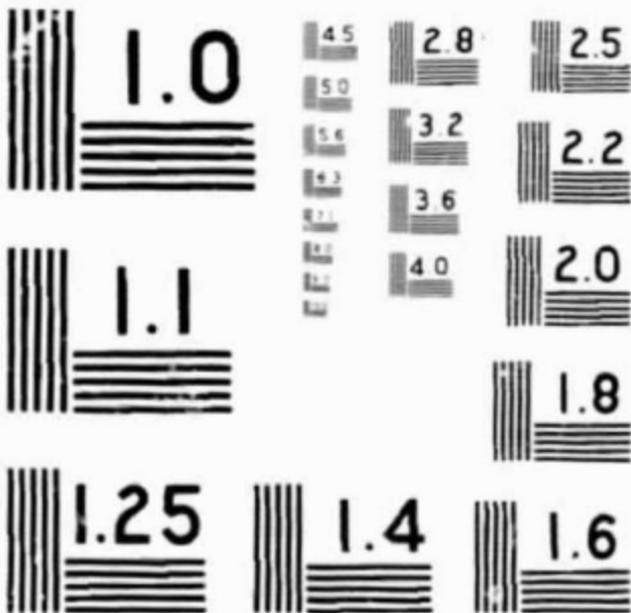
MICROCOPY RESOLUTION TEST CHART
NATIONAL BUREAU OF STANDARDS – 1963
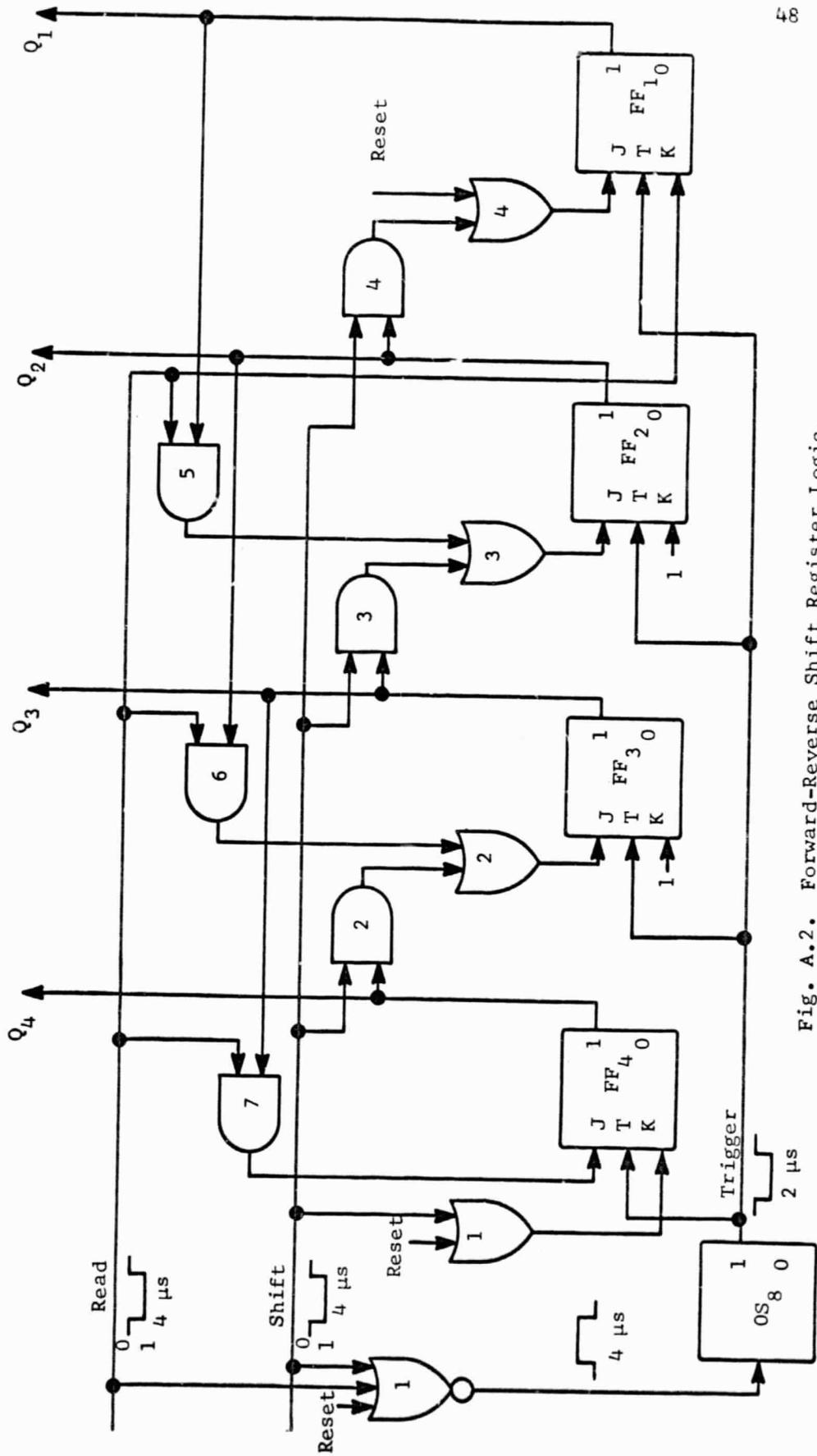
(To BSR and D/A Converter)

Fig. A.2. Forward-Reverse Shift Register Logic.

48

flip-flop. The delay insures that the bits being read into the BSR are stored in the correct location before the Q-lines change states.

A.3 QUEUE-ERROR SENSE CIRCUIT

The circuit used to obtain the queue-error voltage from the location of the FRSR reference bit is illustrated in Fig. A.3. It can be noted from the input-output relations tabulated in Table A.1 that the D/A output is equal to a fraction of the reference voltage, e_r, and is directly proportional to the location of the reference bit.

TABLE A.1

CONTROL LOOP D/A CONVERTER INPUT-OUTPUT RELATIONS

Reference Bit Location	D/A Converter Input	D/A Converter Output	Compensator Network Input
Q_4	1001	$3e_r/5$	$+ 3e_r/10$
Q_3	0110	$2e_r/5$	$+ e_r/10$
Q_2	0011	$e_r/5$	$- e_r/10$
Q_1	0000	0	$- 3e_r/10$

Since the BSR has five stages, the queue-error voltage should be 0 V when 2.5 words are stored in the buffer. Hence, a bias voltage is summed with the converter output so that the average input voltage to the compensator network is 0 V when the reference bit oscillates between Q_2 and Q_3. The compensator network output voltage controls the frequency of the VCO, which has output voltage levels compatible with the logic. During the RESET mode, a logic ZERO on $NAND_4$ disables the VCO output so that SHIFT pulses are not applied to the BSR or FRSR.
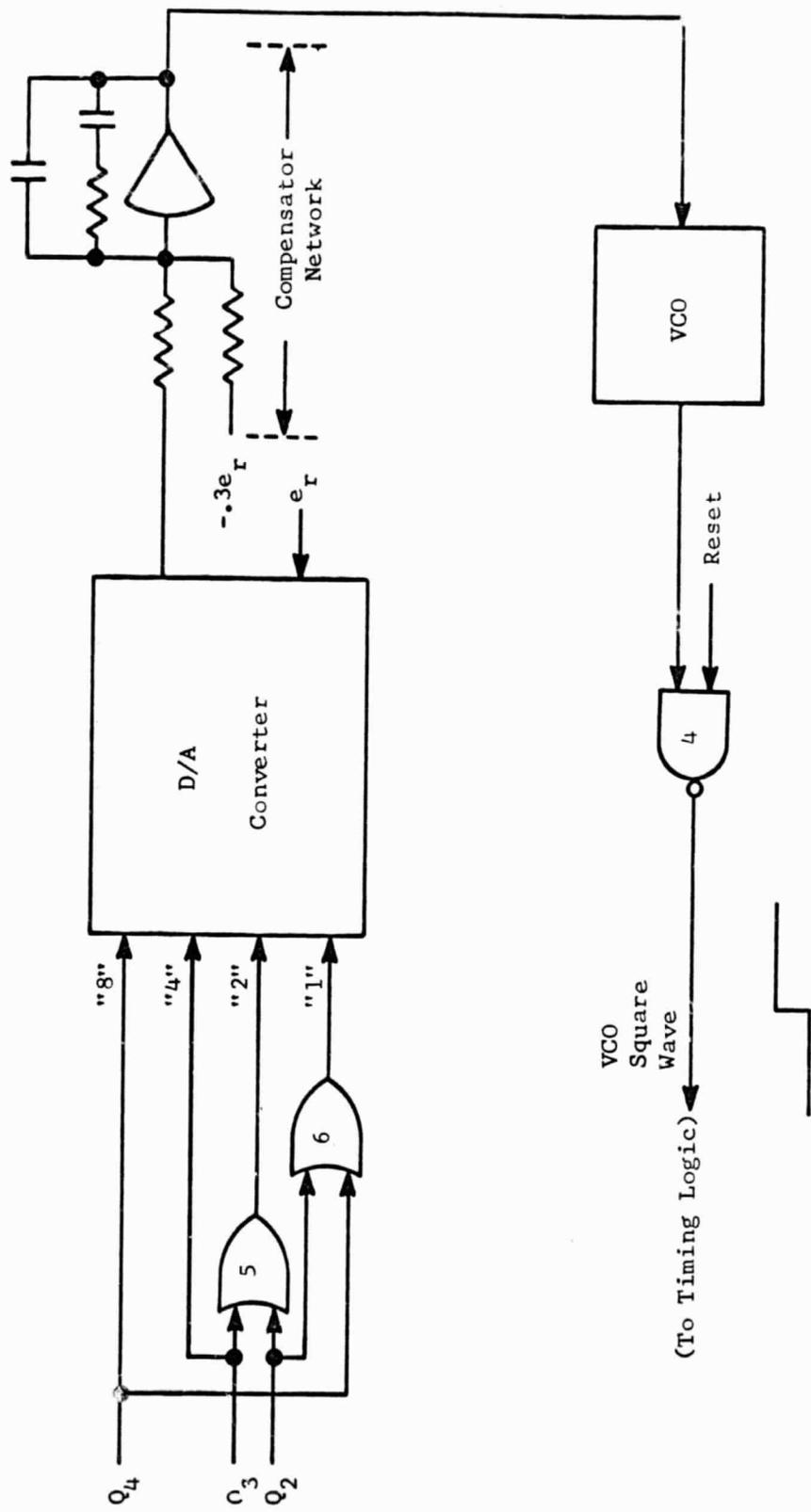
Fig. A.3. Queue-Error Sense Circuit.

A.4 TIMING LOGIC

The timing logic shown in Fig. A.4 is required to prevent simultaneous application of READ and SHIFT pulses to either the BSR or FRSR. All of the pulse widths shown in this figure are chosen for a system with 100 kHz pulse-repetition-rate logic.

A SHIFT pulse is generated 10 μs after each positive going transition of the VCO square wave. A READ pulse is generated for each EOC (end-of-conversion) pulse with a time delay determined by the state of OS_5. The need for this delay is evident from an inspection of Fig. A.5. The level transitions for the VCO, OS_5 gate, and SHIFT pulse waveforms occur at a relatively uniform rate; whereas, the EOC pulse rate varies directly with the flutter of the recorder. Consequently, it is possible for the EOC and SHIFT pulses to overlap or even occur simultaneously. However, the switching speed of the logic requires a minimum time, λ, between the leading edges of the READ and SHIFT pulses. Hence, the EOC pulse must be delayed if it occurs during the ON time of OS_5, which is an interval of 2λ seconds centered about the leading edge of the SHIFT pulse.

Timing diagrams illustrating the operation of the logic for three possible locations of the EOC pulse are shown in Fig. A.6. Case 1 occurs when the leading edge of the EOC pulse is not within the 2λ interval of OS_5. The EOC pulse is passed by the circuit consisting of $NAND_1$, OS_1, and $NAND_3$ to generate the READ pulse without delay, neglecting the logic switching delay. The ZERO level of OS_2 disables AND_1 so that the pulse transmitted by $NAND_2$ and OS_3 will be prevented from generating a second READ pulse. Case 2 occurs when the complete EOC pulse is within the 2λ interval. Since $NAND_1$ is disabled by the ZERO

Fig. A.4. Timing Logic.

53

VCO

OS$_5$
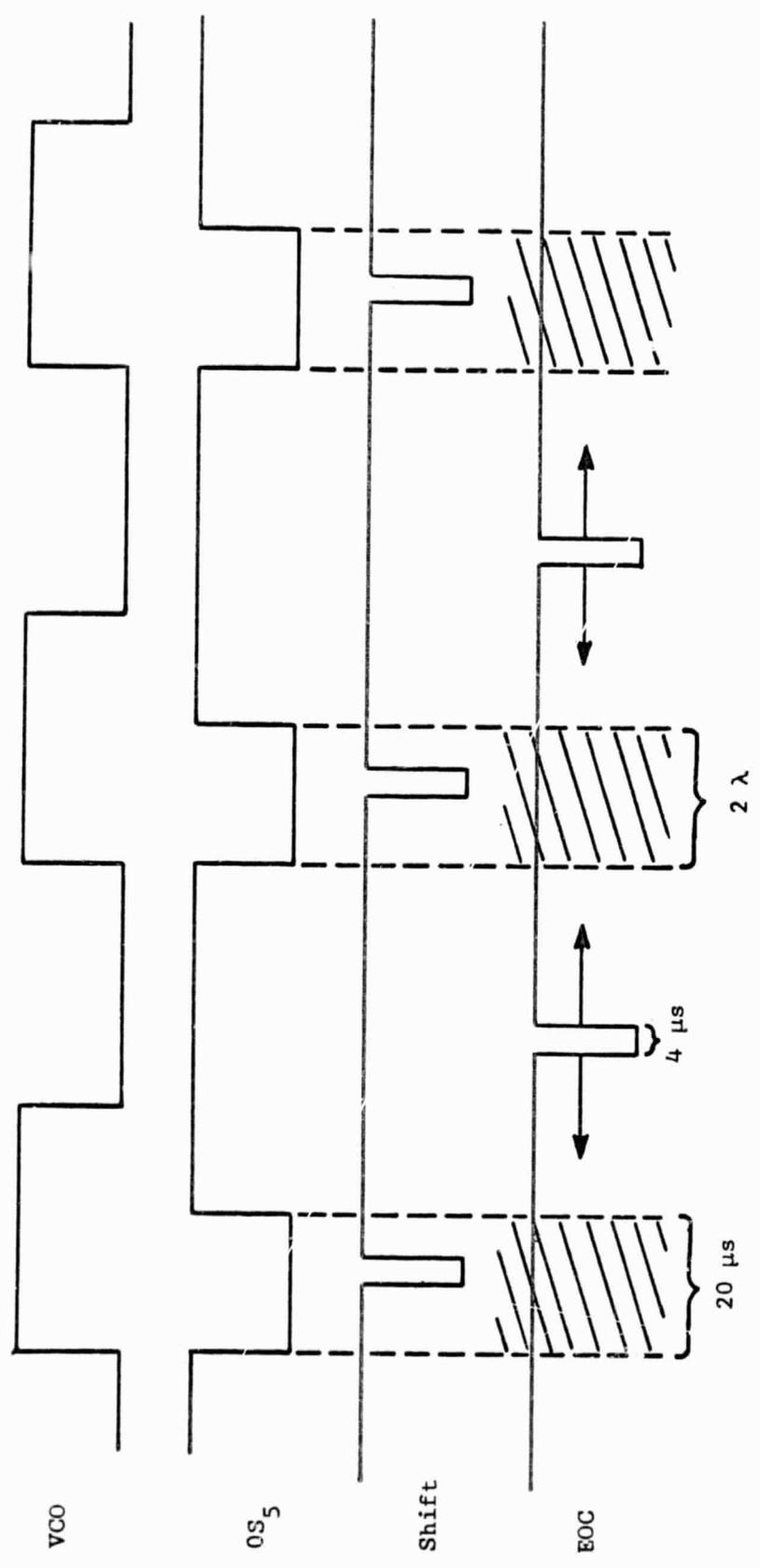
Shift

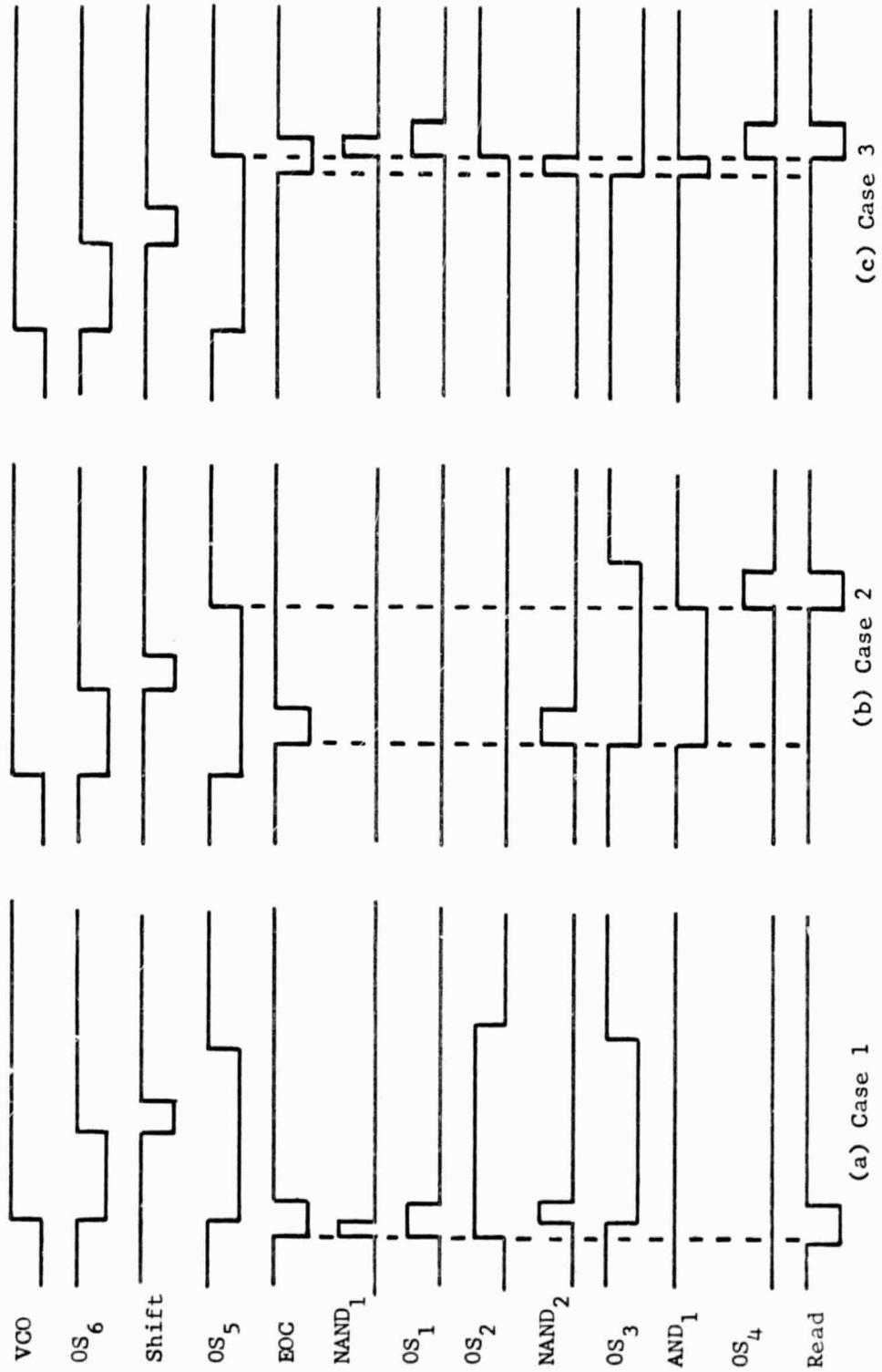EOC

20 μs

4 μs

2 λ
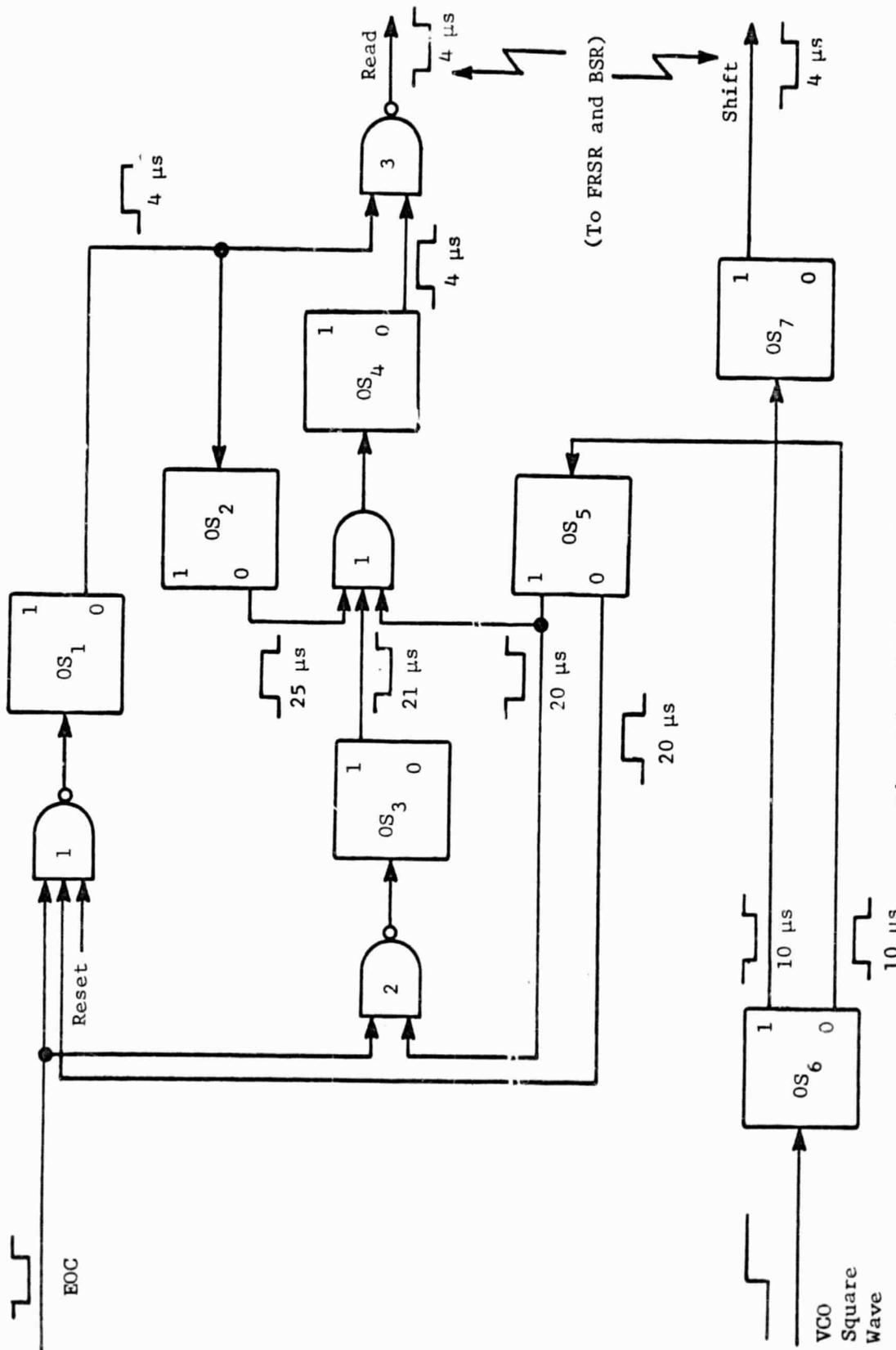
Fig. A.5. Timing Limitation.

54

Fig. A.6. Timing Diagrams for Timing Logic.

(a) Case 1

(b) Case 2

(c) Case 3

VCO

OS_6

Shift

OS_5

EOC

$NAND_1$

OS_1

OS_2

$NAND_2$

OS_3

AND_1

OS_4

Read

output of OS_5, the EOC pulse must be passed through $NAND_2$ and OS_3. The pulse is delayed until the 1-output of OS_5 changes state to a ZERO, which is 10 μs after the leading edge of the SHIFT pulse. At this time the output of AND_1 triggers OS_4 to generate the READ pulse. Case 3 occurs when only the leading edge of the EOC pulse is within the 2λ interval. The overlap of the OS_5 gate and the EOC pulse results in a pulse being passed through each of the aforementioned circuits. However, it can be seen by comparing the outputs of OS_1 and OS_4 that both pulses will coincide since the one-shots are both triggered by the positive going transition of OS_5 through $NAND_1$ and AND_1. The delayed pulse again occurs 10 μs after the leading edge of the SHIFT pulse.

A relationship between maximum logic switching speed, 1/λ, and maximum pilot signal frequency can be determined by considering the timing relations of Case 2. If the EOC pulse occurs slightly after the positive transition of the VCO wave, the corresponding READ pulse will occur 2λ seconds later. After this READ pulse, there must be another λ seconds before the next READ or SHIFT pulse occurs. Consequently, the next EOC pulse cannot occur until λ seconds after the delayed READ pulse. Hence, the total time required between EOC pulses is 3λ. Any other location of the EOC pulse with respect to the VCO wave results in less required time between EOC pulses. Since the EOC pulse rate is numerically equal to the pilot signal frequency, the maximum frequency of the pilot signal is 1/3λ. For example, the pilot signal for a system with 100 kHz logic would be limited to an instantaneous frequency of 33.3 kHz, including the frequency deviation due to recorder flutter.

The number and type [15] of integrated circuit modules required for a digital recorder compensation system with a five stage buffer are tabulated in Table A.2. All logic gate functions have been implemented with NAND circuits and a crystal oscillator [16] has been used for the VCO. Discrete circuit components such as resistors and capacitors have not been listed for the operational amplifier, VCO, and one-shots. If these are included the total cost for system components should be approximately $500.

All of the IC's and discrete components, with the exception of the D/A converter and driver, can be mounted on one 4 3/4" x 4" printed circuit card by assembling the IC's in interconnected layers. Another card would be required for the discrete components of the D/A converter and driver. The total weight of the IC's is less than 1 oz and each card including discrete components weighs approximately 3 ozs. Hence, the total weight for the system components should be less than 8 ozs. It is estimated that approximately 19 in^3 would be required for the system if the components and boards were encapsulated with a filling material.

TABLE A.2

INTEGRATED CIRCUIT SYSTEM

COMPONENTS AND COST

	IC MODULES REQUIRED	COST PER MODULE	SUBTOTAL COST
Buffer Shift Register:			
5 flip-flops	5 DTµL 948	$10.25	$51.25
4 2-input NAND gates	1 DTµL 946	13.00	13.00
Forward-Reverse Shift Register:			
4 flip-flops	4 DTµL 948	10.25	41.00
11 2-input NAND gates	3 DTµL 946	13.00	39.00
1 3-input NAND gate	1 DTµL 962	15.00	15.00
1 one-shot	1 DTµL 951	24.50	24.50
Timing Logic:			
7 one-shots	7 DTµL 951	24.50	171.50
2 3-input NAND gates	(2 available from FRSR)		
3 2-input NAND gates	1 DTµL 946	13.00	13.00
Control Logic:			
3 2-input NAND gates	1 DTµL 946	13.00	13.00
1 operational amplifier	1 µA709	10.00	10.00
1 RF/IF amplifier (VCC)	1 µA703	10.00	10.00
1 comparator (VCO)	1 µA710	10.00	10.00
1 4 bit D/A converter driver	1 IDA-0255*	24.75	24.75
1 4 bit D/A converter	1 IDA-9001*	54.20	54.20
		TOTAL	$490.20

---

*Discrete component circuits

APPENDIX B

FREQUENCY LIMITATIONS OF EXPERIMENTAL RESULTS

The experimental results of this study were obtained by measuring the instantaneous frequency deviation of FM modulated sinusoids with a DCS Model GSD-5 discriminator. The modulated signals were the input and output data signals which had carrier frequencies of 1.3 kHz and the control loop VCO and pilot signals which had carrier frequencies of 14.3 kHz.

Since bandpass filters having standard IRIG [17] center frequencies and bandwidths were used in the discriminator, the bandwidths of the modulated frequency spectra were restricted to IRIG values to prevent distortion due to attenuation of spectral sidebands. The maximum permissible values were used. These values were obtained for sinusoidal modulation by calculating the bandwidths required to pass all components of the FM frequency spectra having relative amplitudes greater than 0.01 [18] . The results are plotted in Figs. B.1 and B.2 as a function of the modulating signal frequency and amplitude, E_m. Also indicated on each plot is the $\pm$ 7.5% bandwidth limit of the appropriate discriminator bandpass filter. The curves of Fig. B.1 were used to determine allowable combinations of amplitude and frequency for the modulation of the 1.3 kHz carriers and the curves of Fig. B.2 were used in a similar manner for the 14.3 kHz carriers.

Narrow-Band
FM Approximation

Discriminator Bandwidth
(1.3 kHz B. P. Filter)

$E_m = 1.0$ v

$E_m = 0.5$ v

$E_m = 0.25$ v

$E_m = 0.1$ v

Wide-Band
FM Approximation

MODULATION FREQUENCY (Hz)

1000

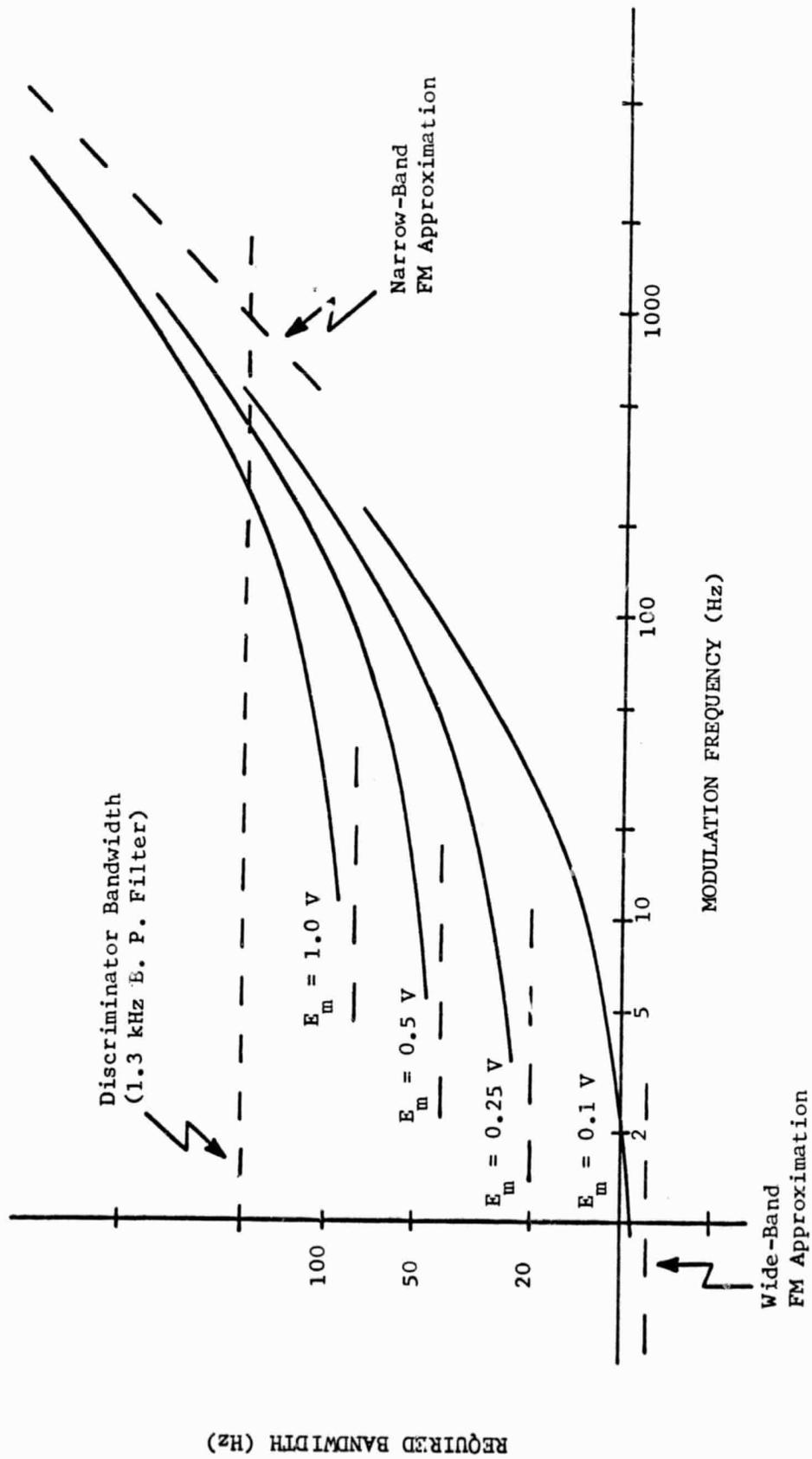100

10

5

2

100

50

20

REQUIRED BANDWIDTH (Hz)

Fig. B.1. Bandwidth Required for a Sinusoidal
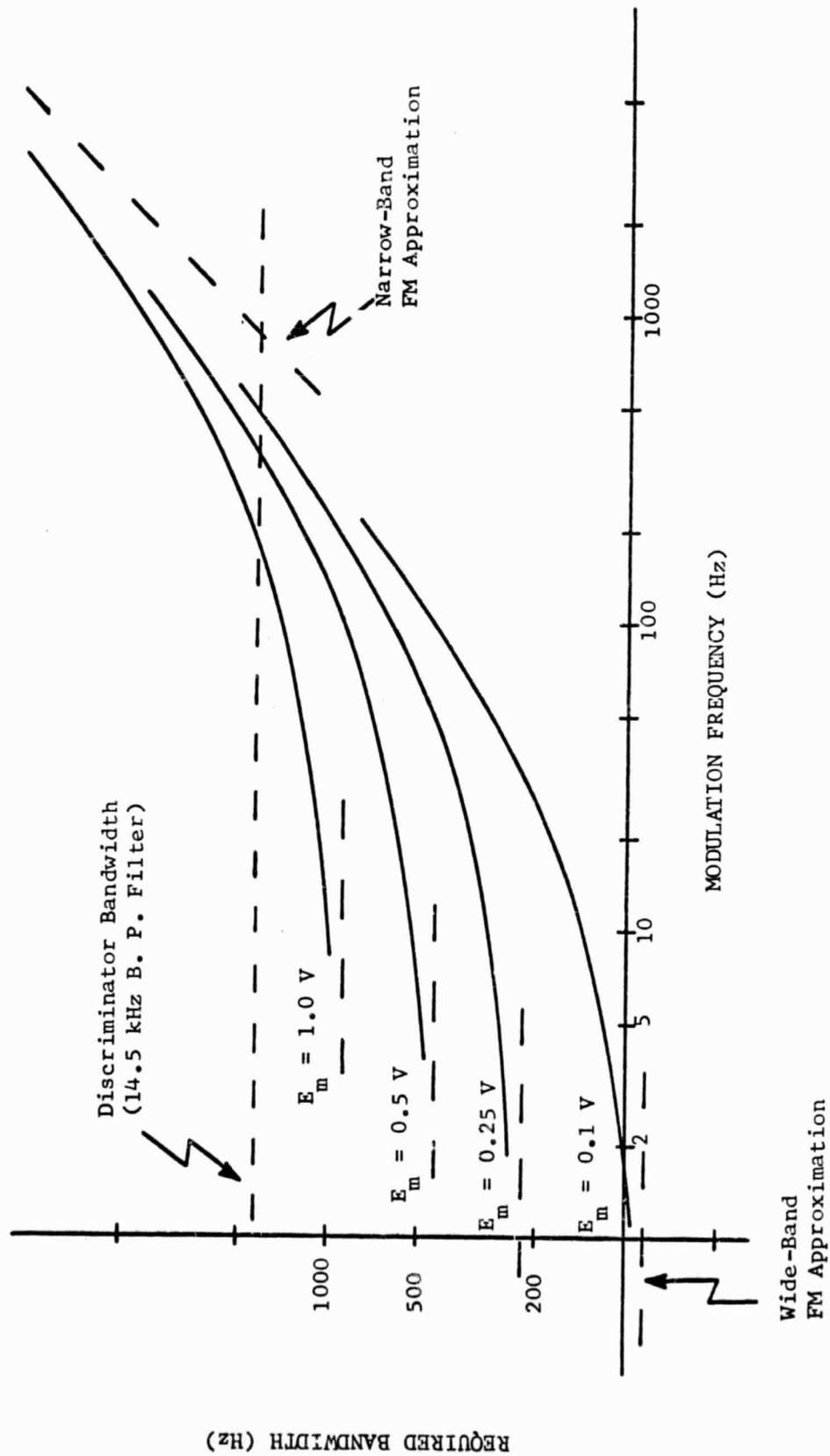Modulated Carrier, $\Delta\omega_c = 40 \ E_m$.

60

Fig. B.2. Bandwidth Required for a Sinusoidal Modulated Carrier, $\Delta\omega_c = 440\ E_m$.

APPENDIX C

DESIGN EXAMPLE

A data signal having spectral components up to 1.3 kHz, is to be recorded on a magnetic tape recorder. Suppose the recorder has a flat flutter power spectrum which extends from $\omega_a = 125$ to $\omega_b = 825$ and a rms flutter of 4.3×10^{-3}. The flutter power density, given by (1.14), is

$$G_o = 1.66 \times 10^{-7} \text{ /Hz.} \tag{C.1}$$

The rms TBE, given by (1.18), is

$$\sigma_h = 13.4 \ \mu s. \tag{C.2}$$

The relatively high magnitude of TBE and the low-frequency components in the flutter power spectrum indicate that the tape recorder being considered has an inefficient speed servo. Consequently, some degree of electronic compensation is desired to reduce the TBE in the recorder output. Such compensation can be achieved by designing the system to meet certain specifications. A typical set of specifications are the following:

(1) The compensation system must attenuate all frequency components of TBE by a minimum of 18 dB.

(2) The TBE attenuation rate should be at least 12 dB/octave.

(3) The frequency at which any peak in the TBE attenuation characteristic occurs should be at least two octaves below the lowest frequency component of TBE.

(4) Any peak in the attenuation characteristic should be less than 1.6.

(5) The phase margin of the system should be at least 40°.

(6) The probability of any data loss should not be greater than 10^{-6}.

These specifications will be used as the basis to design a compensator network, to choose the loop gain, and to determine the required buffer capacity for the digital system presented in Chapter 3.

The Bode design procedure $\left[19\right]$ will be used to determine the compensator network and loop gain. The Bode diagram will be drawn for the uncompensated system, the design specifications will be converted to limitations on the Bode diagram, and a compensator network and loop gain will be choosen so that the limitations are satisfied. The buffer capacity will be determined from Specification (6) which defines the acceptable probability of buffer overflow or underflow.

The first four specifications define the shape of the required TBE attenuation characteristic. They can put in a more meaningful form by using (2.17) to directly translate each of the TBE specifications to a requirement on the rate frequency response, $H_1(j\omega)$; e.g., the first specification requires that

$$\left| H_1(j\omega) \right| \leq 0.125, \qquad (C.3)$$

for $125 < \omega < 825$.

The Bode diagram is the magnitude of the open-loop gain function, $A(j\omega)$, which is defined by

$$H_1(j\omega) = \frac{A(j\omega)}{1 + A(j\omega)}. \qquad (C.4)$$

The Bode diagram for the digital system is determined by comparing (2.10)

and (C.4) and solving for $A(j\omega)$.

$$\left| A(j\omega) \right| = \left| \frac{KG_c(j\omega)}{j\omega} \right| \quad , \tag{C.5}$$

which is plotted in Fig. C.1 for $K = 100$ and $G_c(j\omega) = 1$. The magnitude of the open-loop gain function is small for high frequencies, so the closed-loop frequency response magnitude, $\left| H_1(j\omega) \right|$, can be approximated by the Bode plot, $\left| A(j\omega) \right|$. The first specification, given by (C.3), is denoted by the asterisk (*) at $\omega = 125$ on Fig. C.1. This specification could be satisfied by reducing the loop gain to $K = 16$ as indicated by the dashed line.

The second specification requires that the attenuation rate of $\left| H_1(j\omega) \right|$ be at least 12 dB/octave for $\omega > 125$. The purpose of this specification is to insure that there is a significant reduction in the power contained in the TBE power spectrum at the output of the system. Specification (2) cannot be satisfied by changing the loop gain, since the slope of the uncompensated Bode plot is -6 dB/octave* for all frequencies. However, a compensator network can be chosen such that the Bode plot for the resulting system has a high frequency atten-uation greater than 6 dB/octave. Some typical compensator network transfer functions are the following:

$$G_{c_1}(s) = \frac{1}{\tau_1 s + 1} \quad , \tag{C.6}$$

$$G_{c_2}(s) = \frac{\tau_2 s + 1}{(\tau_1 s + 1)(\tau_3 s + 1)} \quad , \tag{C.7}$$

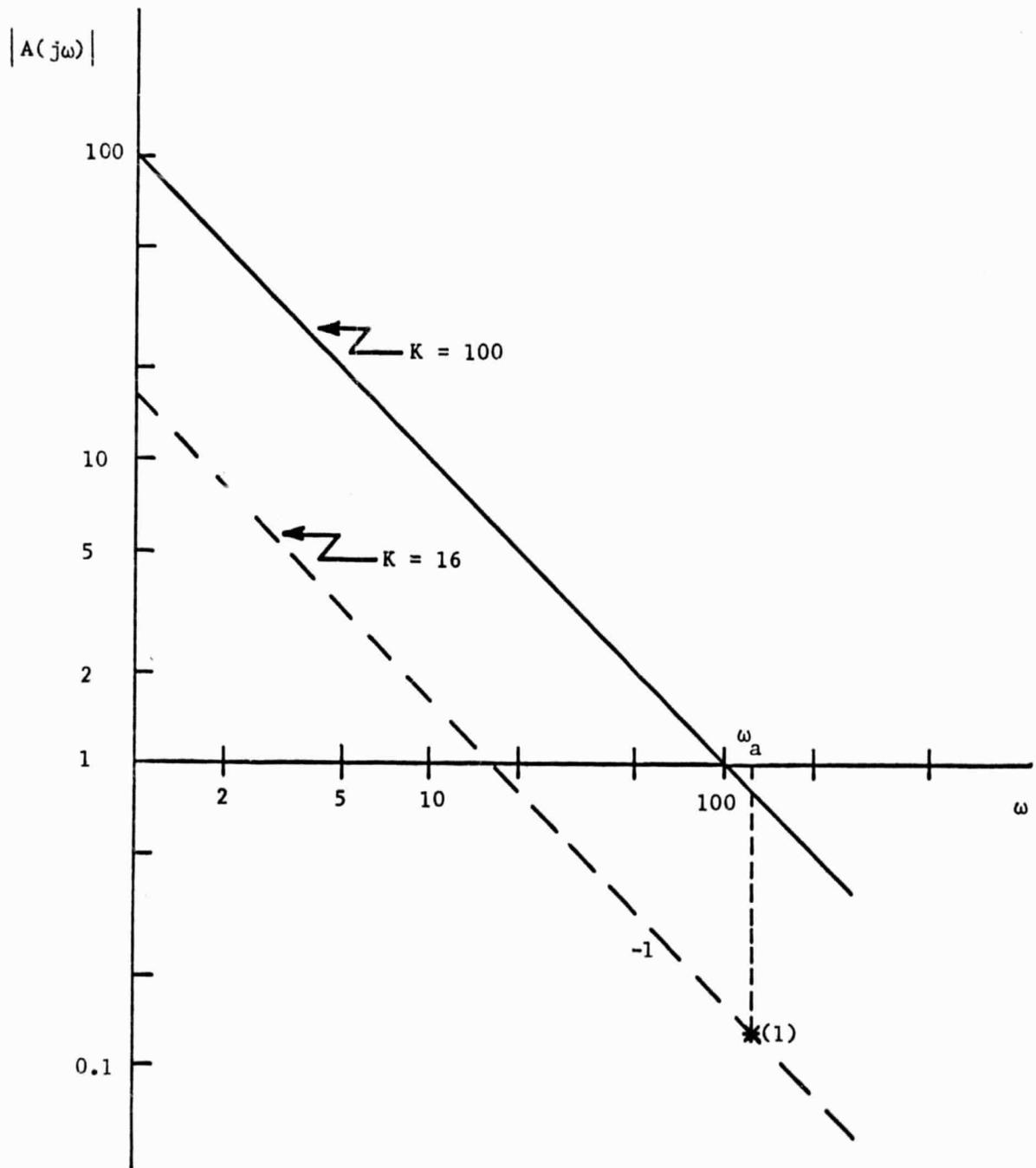*Slopes of -6dB/octave and -12 dB/octave will be indicated on all Bode diagrams by -1 and -2 respectively.

Fig. C.1. Bode Diagram for System
without Compensator Network.

and

$$G_{c_3}(s) = \frac{\tau_1 s + 1}{s(\tau_2 s + 1)} \, . \tag{C.8}$$

The Bode plot of the system with each one of these compensators is sketched in Fig. C.2.

A compensator with a transfer function of the form given by (C.8) has a definite advantage, which can be seen by considering the queue-error transfer function, $H_2(s)$, given by (2.11). The static change in $q_e(t)$ due to a static change of $d_i(t) = D$ in the input rate can be found by applying the final-value theorem,

$$q_{ss}(t) = \lim_{s \to 0} s \left[H_2(s) \right] \frac{D}{s} \, . \tag{C.9}$$

The transfer function of $G_{c_3}(s)$ is the only one of the three to give a system with a zero steady state queue-error. By choosing this type of compensator network, none of the buffer storage capability needs to be allotted to frequency drifts of the pilot signal or control loop VCO.

The parameters τ_1, τ_2, and K must now be determined to complete the control-loop design. Specifications (3) and (4) are maximum limits on the frequency, ω_m, and magnitude, M_p, of any peak in $\left| H_1(j\omega) \right|$. The TBE of the data signal can be increased by the system if the tape recorder has unmeasured flutter spectral components with frequencies near ω_m. Hence, the M_p and ω_m specifications minimize the effects of any errors in the measurement of the lower limit of the flutter spectrum.

Specification (3) limits ω_m to a frequency which is two octaves below $\omega_a = 125$, i.e.,

$$\omega_m \leq 31.25. \tag{C.10}$$

The frequency at which the Bode diagram crosses the unity gain axis,
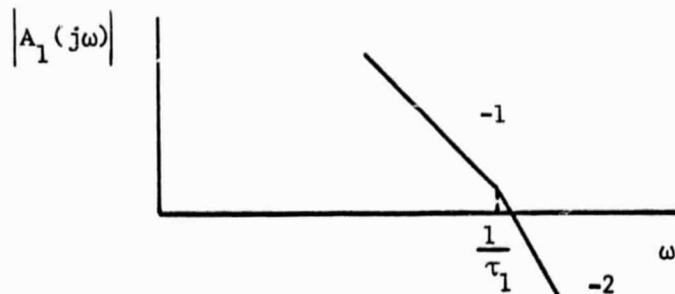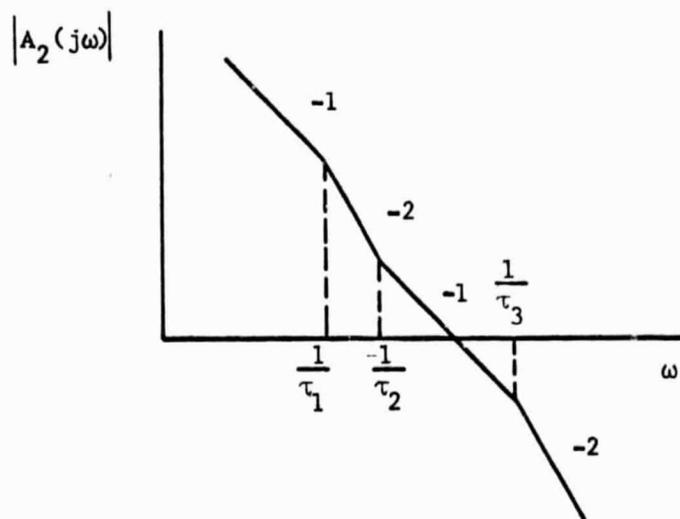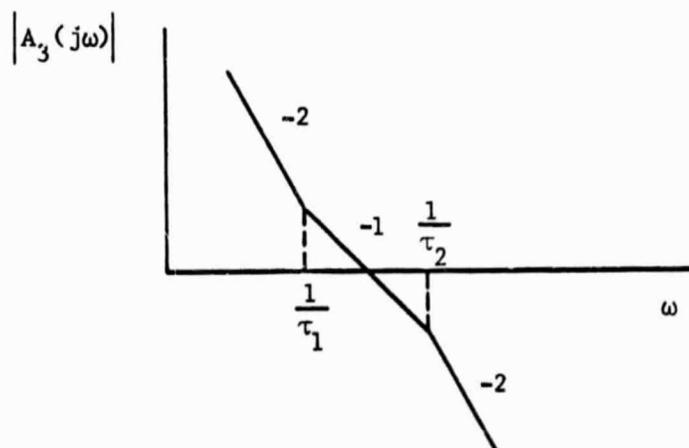
(a) Lag Compensator Network, $G_{c_1}(s)$

(b) Lag-Lead-Lag Compensator Network, $G_{c_2}(s)$

(c) Integrator Compensator Network, $G_{c_3}(s)$

Fig. C.2. Bode Diagram for System Employing Various Compensator Networks.

β_c, is normally greater than ω_m so Specification (3) will be satisfied if

$$\beta_c \leq 31.25, \tag{C.11}$$

which is denoted by the asterisk on Fig. C.3 at $\omega = 31.25$. Two portions of the Bode diagram have been drawn through the Specifications (1) and (3) limit points, and the intersection of these two lines define

$$\frac{1}{\tau_2} = 60. \tag{C.12}$$

The dashed lines show the remaining portion of the Bode diagram for various $1/\tau_1$ break points, each of which is associated with a particular value of K.

Specification (4),

$$M_p < 1.6, \tag{C.13}$$

gives a necessary condition for the system phase margin, Ψ, i.e.

$$\Psi \geq \sin^{-1} \frac{1}{M_p}. \tag{C.14}$$

Combining (C.13) and (C.14) gives

$$\Psi > 38.7°. \tag{C.15}$$

Since the Specification (5) requirement,

$$\Psi \geq 40°, \tag{C.16}$$

is more restrictive than (C.15), it is used for the system requirement. The phase margin can be obtained from the Bode diagram by using the arc tan approximation [20],

$$\Psi \approx \frac{\pi}{2} - \frac{1}{\beta_c \tau_1} - \beta_c \tau_2. \tag{C.17}$$

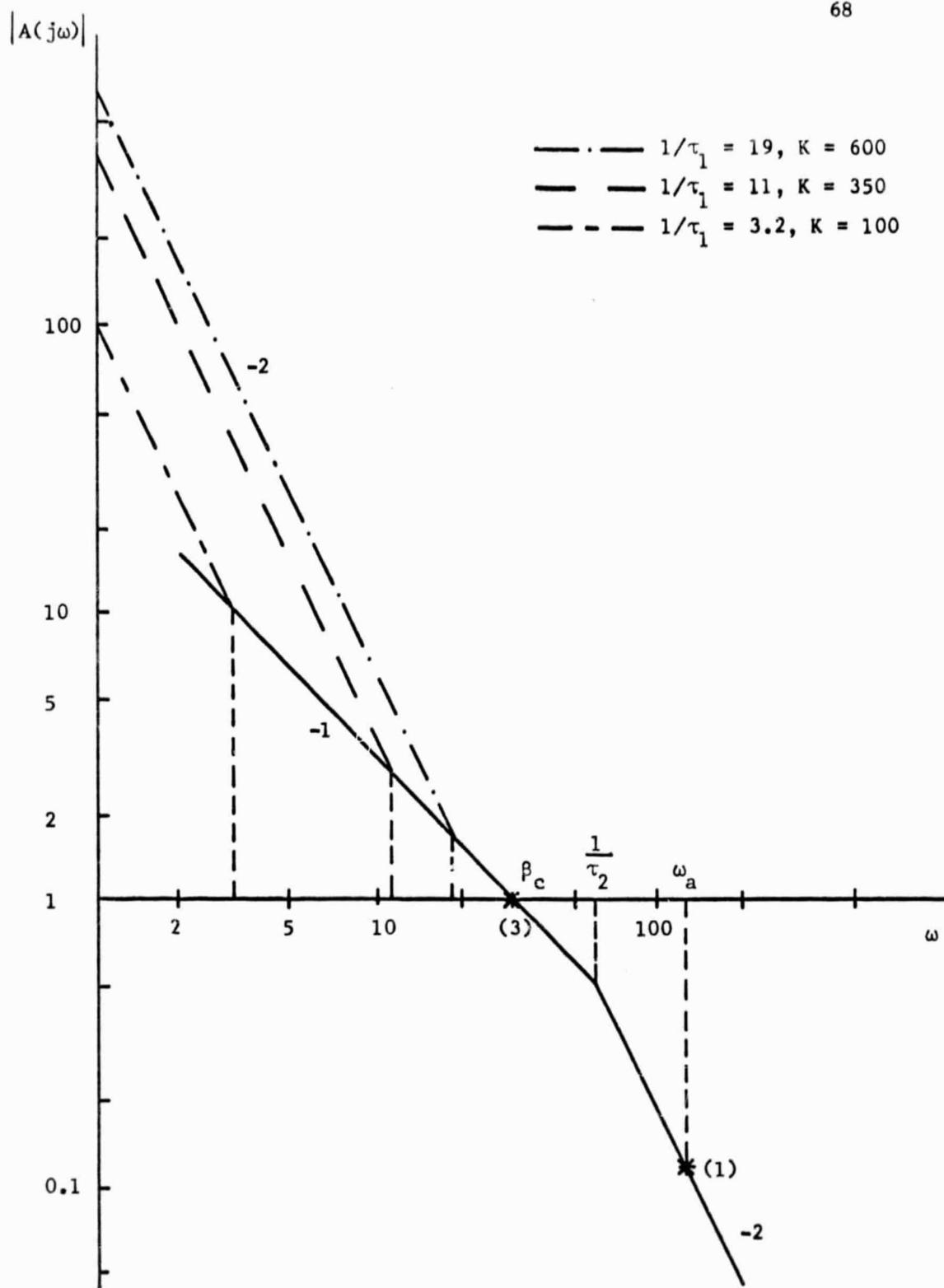Combining the expressions of (C.12), (C.16), and (C.17) with the value

Fig. C.3. Partial Bode Diagram for System with
Integrator Compensator Network.

of β_c = 31.25 from Fig. C.3 yields

$$\frac{1}{\tau_1} \leq 11 \qquad \text{(C.18)}$$

as the limit on the remaining network parameter to be chosen. The corresponding limit on loop gain is

$$K \leq 350. \qquad \text{(C.19)}$$

The choice of the $1/\tau_1$ and K combination is made by considering the effect of gain on the queue-error frequency response, $H_2(j\omega)$. Substituting (C.8) into (2.11) and expressing in terms of ω yields

$$\left| H_2(j\omega) \right| = \left| \frac{-\tau_2\omega^2 + j\omega}{(K-\omega^2)+j(K\tau_1\omega-\tau_2\omega^3)} \right| . \qquad \text{(C.20)}$$

For high frequencies (C.20) gives

$$\left| H_2(j\omega) \right| \approx \frac{1}{\omega} , \qquad \text{(C.21)}$$

which implies that loop gain has no effect. For low frequencies (C.20) gives

$$\left| H_2(j\omega) \right| \approx \frac{\omega}{K} , \qquad \text{(C.22)}$$

which implies that the queue-error will be reduced as K is increased. Hence, the maximum allowable value of K and the corresponding value of $1/\tau_1$, will be used. The compensator network transfer function is then given by (C.8) with the breakpoints defined by (C.12) and (C.18).

$$G_c(s) = \frac{60(s+11)}{11s(s+60)} . \qquad \text{(C.23)}$$

The Bode diagram for (C.23) is given in Fig. C.4 with the diagram for the system, before and after compensation.

A number of approximations have been used in the design of $G_c(s)$. Some of these were the use of the Bode diagram asymptotic approximation,
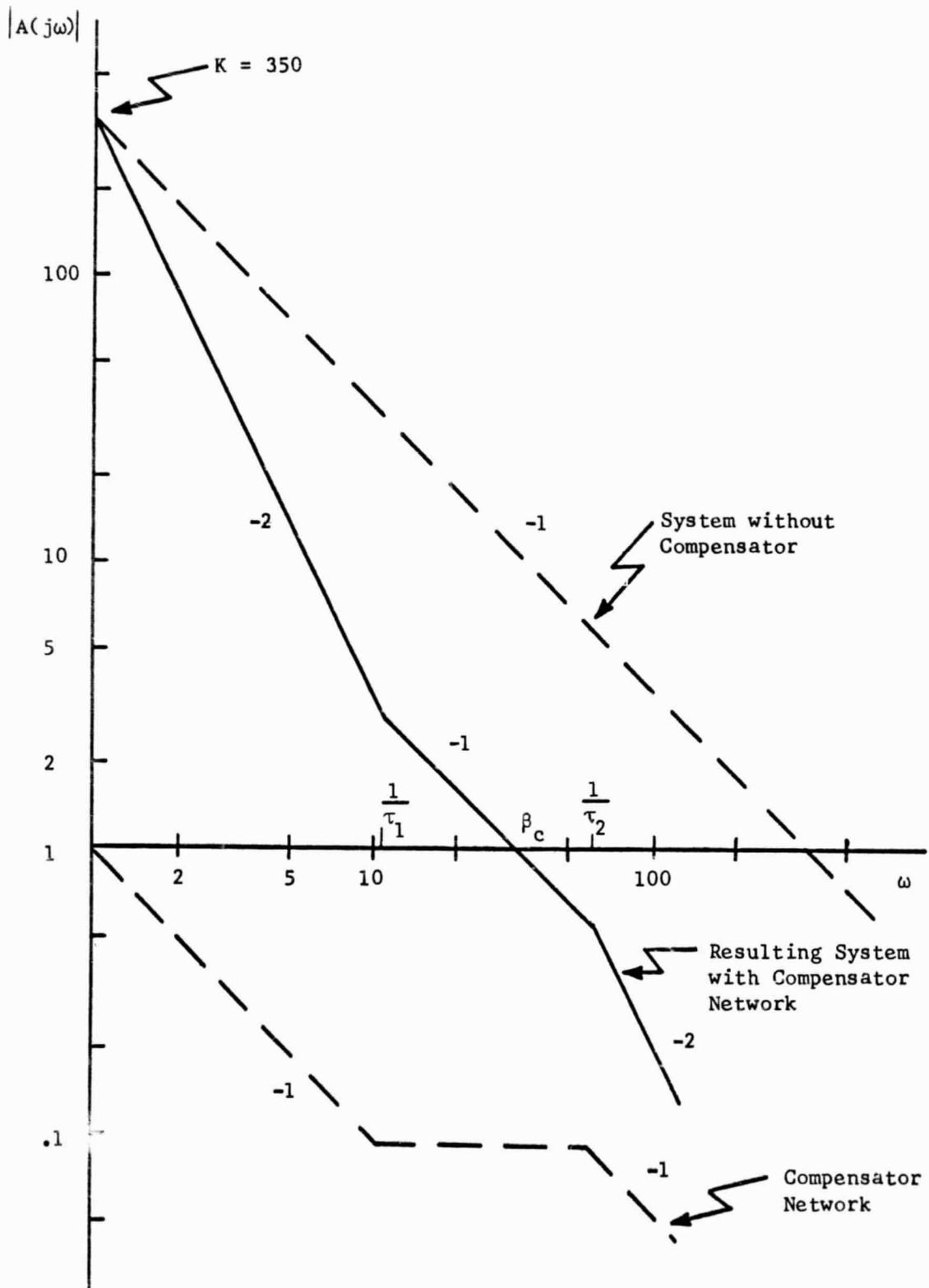
Fig. C.4. Bode Diagram for System with Integrator
Compensator Network.

the necessary but not sufficient condition for M_p, and the arc tan
approximation for Ψ. Thus, the final design must be checked by obtaning
the system Nyquist plot, which is shown in Fig. C.5 with circles of
constant M_p plotted. An inspection of the figure indicates that

$$\omega_m \approx 24, \tag{C.24}$$

$$M_p \approx 1.5, \tag{C.25}$$

and

$$\Psi \approx 43°. \tag{C.26}$$

Comparing these values with the specification requirements shows that
the design is satisfactory.

The transfer function, (C.23), can be synthesized by the active
network given in Fig. C.6 [21] . The component values are defined by

$$B = R_2(C_1 + C_2), \tag{C.27}$$

$$T = R_1 C_2, \tag{C.28}$$

and

$$\theta = \frac{C_1}{C_1 + C_2}, \tag{C.29}$$

where the network transfer function is

$$\frac{E_o(s)}{E_i(s)} = \frac{-(Ts+1)}{Bs(\theta Ts+1)}. \tag{C.30}$$

The next step in the design procedure is to determine the pilot
signal frequency. The highest frequency component in the data signal
is 1.3 kHz. Hence, a 14.3 kHz pilot signal can be used and the data
signal will be sampled at least 11 times for each cycle of its highest
spectral component.

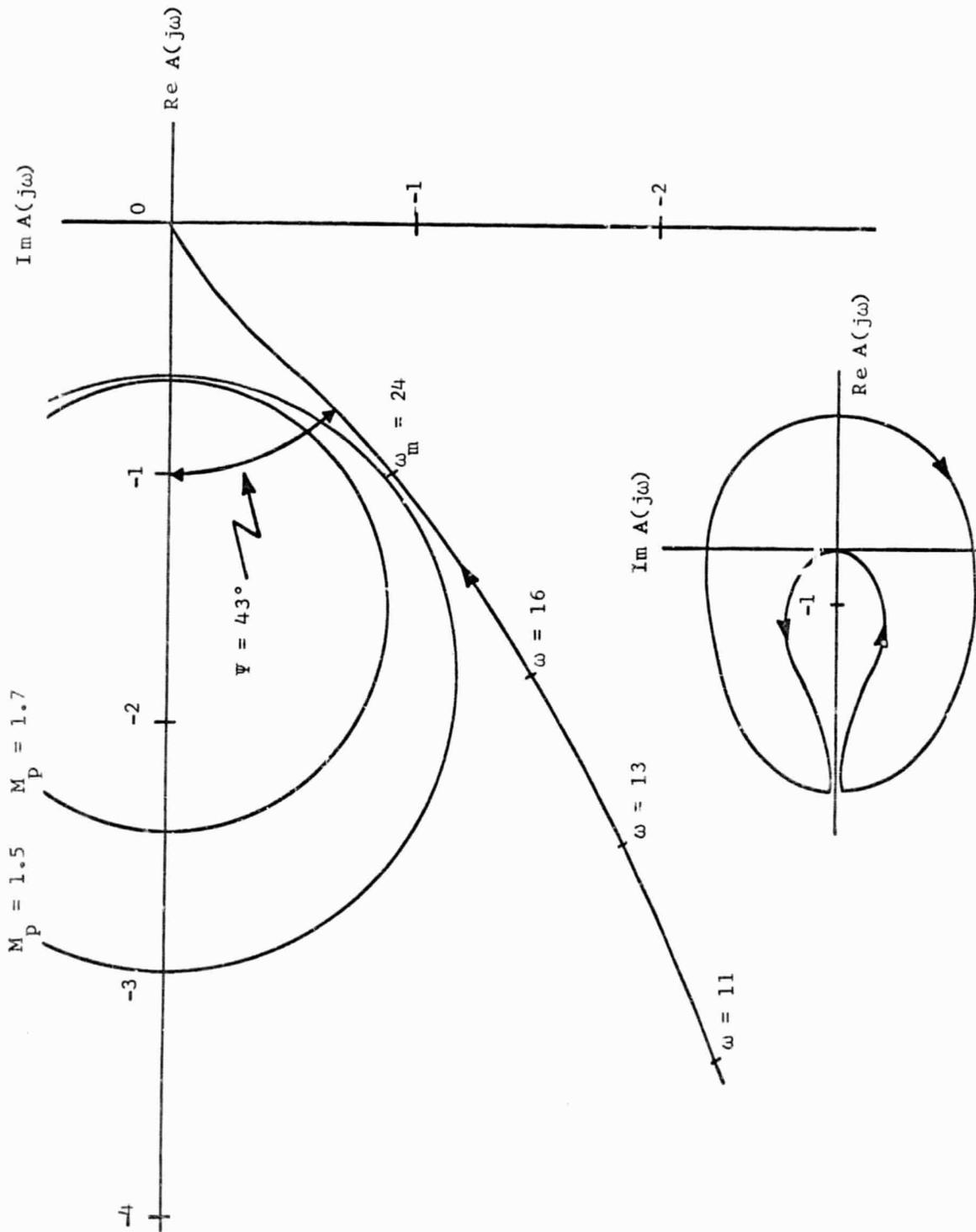The σ_q value is determined by using the expression of Case 4 in

Fig. C.5. Nyquist Plot for System with Integrator Compensator Network.
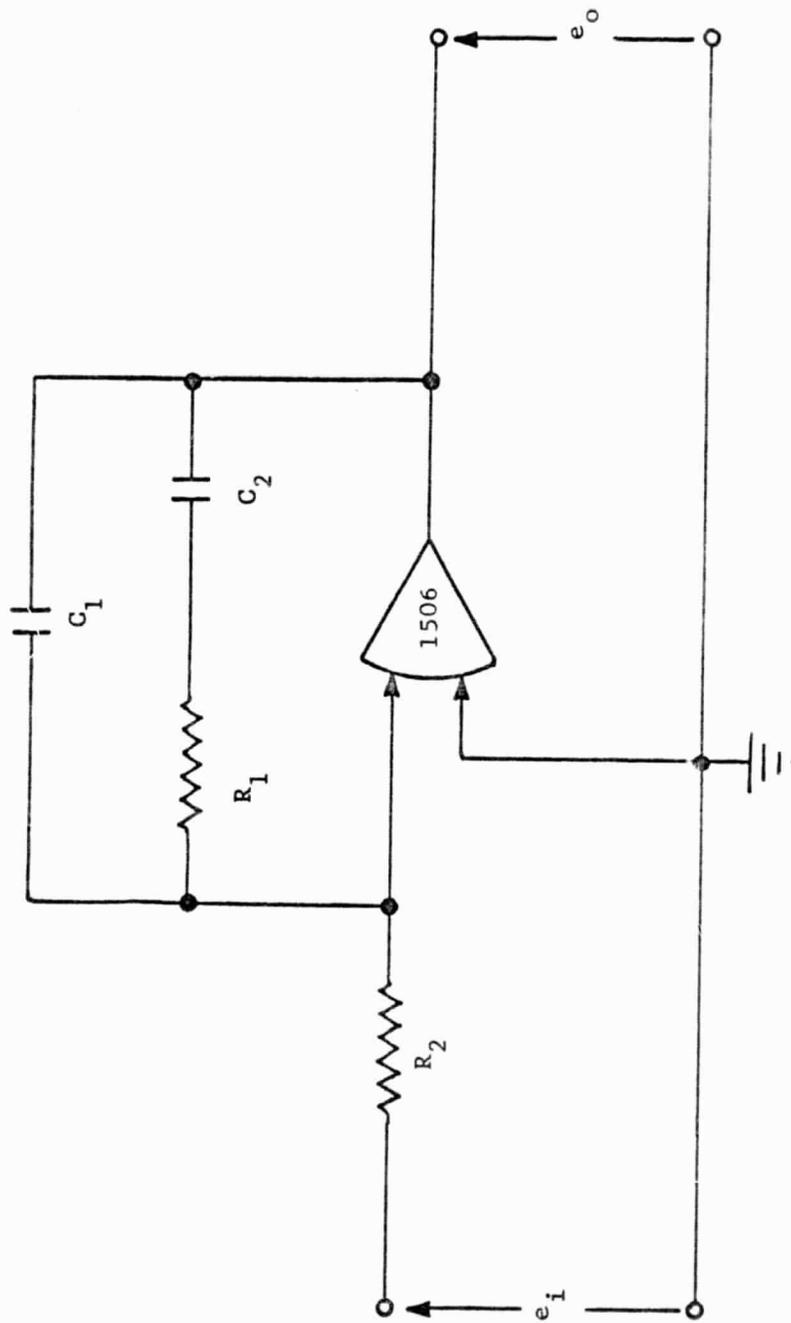
Fig. C.6. Compensator Network.

Table D.1 of Appendix D. Substituting the compensator network, loop gain, and flutter spectral density parameters into this expression along with the mean input rate, R_o = 14.3 kwps gives

$$\sigma_q = 1.0 \text{ word}. \tag{C.31}$$

The final step is to determine the required buffer capacity for the probability of buffer overflow or underflow, $P_{ou}(k)$, as given by Specification (6). The required buffer capacity for an error probability of 10^{-6} is determined by obtaining a value of k from Fig. E.2 and substituting this value and (C.31) into (E.1).

$$C_b = 10 \text{ words}. \tag{C.32}$$

A 10 stage buffer is a conservative design since the results tabulated in Table D.1 are for a uniform flutter spectrum containing all frequencies; whereas, the design flutter spectrum is limited to a bandwidth of 700 rad/s.

APPENDIX D

DERIVATION OF EXPRESSIONS FOR THE QUEUE-ERROR VARIANCE

The variance of queue-error, σ_q^2, is given by

$$\sigma_q^2 = \left\langle q^2(t) \right\rangle - \left\langle q(t) \right\rangle^2, \tag{D.1}$$

where $\left\langle q^2(t) \right\rangle$ is the mean-square queue-error, and $\left\langle q(t) \right\rangle$ is the mean queue-error. The value of $\left\langle q^2(t) \right\rangle$ can be determined from the auto-correlation function, $\phi_q(\tau)$, evaluated at $\tau=0$, i.e.

$$\left\langle q^2(t) \right\rangle = \phi_q(0) = \frac{1}{\pi} \int_0^\infty \Phi_q(\omega) \, d\omega. \tag{D.2}$$

The queue-error power spectrum, $\Phi_q(\omega)$, can be obtained in terms of the transfer function, $H_2(\omega)$, which characterizes the system model.

$$\Phi_q(\omega) = \left| H_2(j\omega) \right|^2 \Phi_{d_i}(\omega). \tag{D.3}$$

The input rate deviation spectrum, $\Phi_{d_i}(\omega)$, can be obtained in terms of the flutter spectrum, $G(\omega)$, from (2.14).

$$\Phi_{d_i}(\omega) = R_o^2 \left| G(\omega) \right|^2. \tag{D.4}$$

Substituting (D.3) and (D.4) into (D.2) yields

$$\left\langle q^2(t) \right\rangle = \frac{R_o^2}{\pi} \int_0^\infty \left| H_2(j\omega) \right|^2 \left| G(\omega) \right|^2 d\omega. \tag{D.5}$$

It follows from (2.14) that

$$\left\langle d_i(t) \right\rangle = R_o \left\langle g(t) \right\rangle = 0, \tag{D.6}$$

since $\left\langle g(t) \right\rangle = 0$. Thus, $q(t)$ has a zero mean since it is the output of a linear system with a zero-mean input. The variance, σ_q^2, can be obtained from (D.1), (D.5) and (2.11).

$$\sigma_q^2 = \frac{R_o^2 G_o}{\pi} \int_0^\infty \left| \frac{1}{j\omega + KG_c(j\omega)} \right|^2 d\omega, \tag{D.7}$$

where it is assumed that the flutter spectrum has a uniform amplitude, $\sqrt{G_o}$.

A procedure for evaluating the integral of (D.7) is illustrated by considering the compensator network transfer function

$$G_c(j\omega) = \frac{(1 + j\tau_1 \omega)}{j\omega(1 + j\tau_2 \omega)} . \tag{D.8}$$

Substituting (D.8) into (D.7) yields

$$\sigma_q^2 = \frac{R_o^2 G_o}{2\pi} \int_{-\infty}^\infty \frac{\left| -\tau_2 \omega^2 + j\omega \right|^2}{\left| K - \omega^2 + j(K\tau_1 \omega - \tau_2 \omega^3) \right|^2} d\omega, \tag{D.9}$$

which can be expressed as

$$\sigma_q^2 = \frac{R_o^2 G_o}{2\pi j} \int_{-j\infty}^{j\infty} \frac{\left[\tau_2 s^2 + s \right] \left[\tau_2 s^2 - s \right] ds}{\left[(s^2 + K) + (\tau_2 s^3 + K\tau_1 s) \right] \left[(s^2 + K) - (\tau_2 s^3 + K\tau_1 s) \right]} \tag{D.10}$$

by making a change of variable to the complex frequency, s, and using a complex number identity. The integral of (D.10) has been evaluated [22] when in the form

$$I = \frac{1}{2\pi j} \int_{-j\infty}^{j\infty} \frac{c(s) \, c(-s) \, ds}{d(s) \, d(-s)} , \tag{D.11}$$

where

$$c(s) = c_2 s^2 + c_1 s + c_o \tag{D.12}$$

and

$$d(s) = d_3 s^3 + d_2 s^2 + d_1 s + d_o . \tag{D.13}$$

The value is

$$I = \frac{c_2{}^2 d_o d_1 + (c_1{}^2 - 2c_o c_2) d_o d_3 + c_o{}^2 d_2 d_3}{2 d_o d_3 (d_1 d_2 - d_o d_3)} \, . \tag{D.14}$$

Hence, comparing (D.10) with (D.11) through (D.14) and simplifying yields

$$\sigma_q{}^2 = R_o{}^2 \frac{G_o (K \tau_1 \tau_2 + 1)}{2K(\tau_1 - \tau_2)} \, . \tag{D.15}$$

Similar results are tabulated in Table D.1 for other common compensator networks. The expressions in the table can only be applied for a network which results in a stable system, since stability is one of the assumptions used to evaluate (D.11).

Table D.1 QUEUE-ERROR VARIANCE FOR VARIOUS
COMPENSATOR NETWORKS

CASE	COMPENSATOR NETWORK $G_c(s)$	NORMALIZED QUEUE-ERROR VARIANCE σ_q^2/R_o^2
1	$\dfrac{1}{\tau_1 s+1}$	$\dfrac{G_o(\tau_1 K+1)}{2K}$
2	$\dfrac{1}{(\tau_1 s+1)(\tau_2 s+1)}$	$\dfrac{G_o\left[K(\tau_1^2+\tau_1\tau_2+\tau_2^2)+\tau_1+\tau_2\right]}{2K\left[(\tau_1+\tau_2)-K\tau_1\tau_2\right]}$
3	$\dfrac{\tau_1 s+1}{s}$	$\dfrac{G_o}{2K\tau_1}$
4	$\dfrac{\tau_1 s+1}{s(\tau_2 s+1)}$	$\dfrac{G_o(K\tau_1\tau_2+1)}{2K(\tau_1-\tau_2)}$
5	$\dfrac{(\tau_1 s+1)(\tau_2 s+1)}{s^2}$	$\dfrac{G_o(\tau_1+\tau_2)}{2\left[K\tau_1\tau_2(\tau_1+\tau_2)-1\right]}$
6	$\dfrac{(\tau_1 s+1)(\tau_2 s+1)}{s^2(\tau_3 s+1)}$	$\dfrac{G_o\left[K\tau_1\tau_2\tau_3(\tau_1+\tau_2)+\tau_1+\tau_2-\tau_3\right]}{2\left[K\tau_1\tau_2(\tau_1+\tau_2)-K\tau_3(\tau_1+\tau_2)^2-1\right]}$

APPENDIX E

SPECIFICATION OF BUFFER CAPACITY

The required buffer capacity is defined by [23]

$$C_b = k\ \sigma_q,$$ (E.1)

where k is a constant determined by the desired probability of buffer underflow or overflow, $P_{ou}(k)$. The probability of underflow or overflow can be expressed, using (2.3), as the probability that $\left| q_e(t) \right| > C_b/2$.

Since $q_e(t)$ is a normally distributed variable with zero mean and variance σ_q^2, its probability density function, $p_q(\lambda)$, is given by

$$p_q(\lambda) = \frac{1}{\sigma_q \sqrt{2\pi}}\ e^{-\lambda^2/2\sigma_q^2},$$ (E.2)
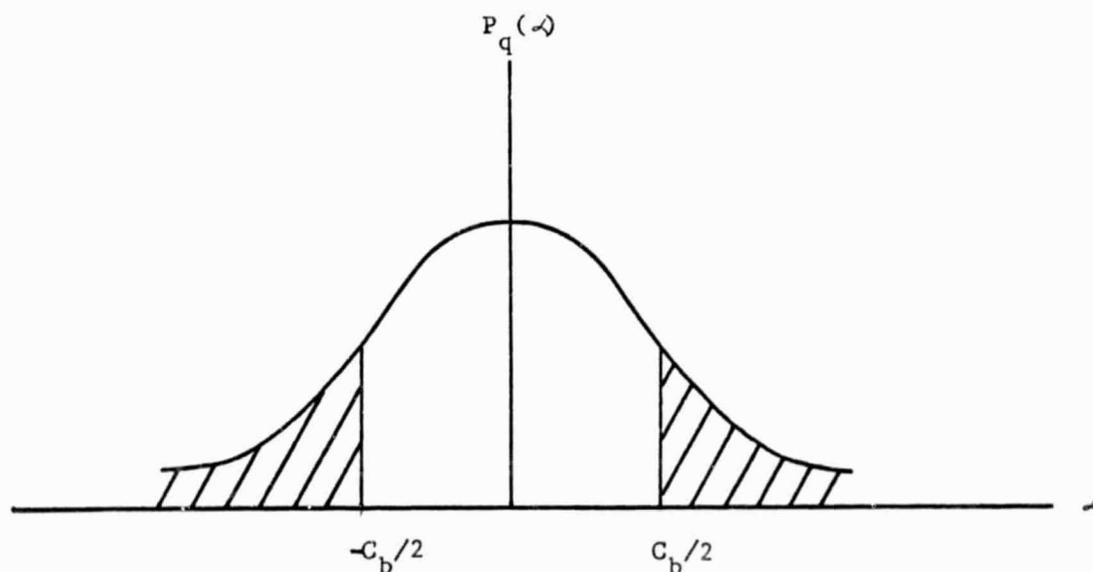
which is plotted in Fig. E.1.

Fig. E.1. Queue-Error Distribution.

The shaded area equals the probability of underflow or overflow, i.e.,

$$P_{ou}(k) = P\left(\left|q_e(t)\right| > C_b/2\right)$$

$$= 2 \int_{-\infty}^{-C_b/2} p_q(\alpha)\, d\alpha. \qquad (E.3)$$

Substituting (E.2) into (E.3) yields

$$P_{ou}(k) = 1 - \operatorname{erf}\left(\frac{C_b}{2\sqrt{2}\,\sigma_q}\right). \qquad (E.4)$$

Substituting (E.1) into (E.4) gives

$$P_{ou}(k) = 1 - \operatorname{erf}(k/\sqrt{8}), \qquad (E.5)$$

which is plotted as a function of k in Fig. E.2. For any given $P_{ou}(k)$, a corresponding value of k is determined from the figure and is substituted into (E.1) to give the required buffer capacity.
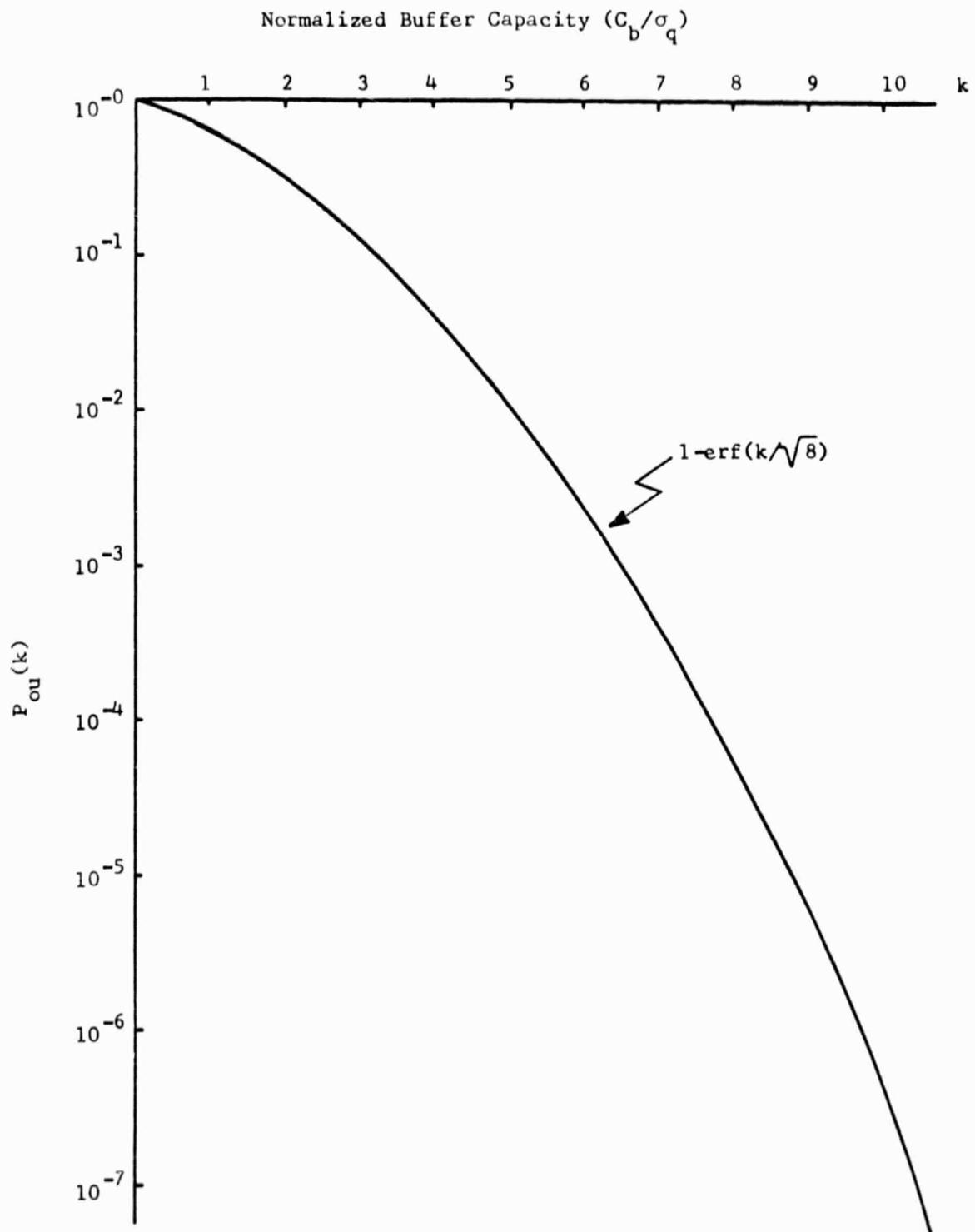
Fig. E.2. Probability of Buffer Overflow or Underflow.

APPENDIX F

TAPE RECORDER SIMULATION

The tape recorder described in the design example was simulated
by the technique shown in Fig. F.1 in order to verify the experimental
performance of the digital system. The VCO gains, K_v, for the data
and pilot signal were -40 Hz/V and -440 Hz/V respectively and their
instantaneous output frequencies are given by the relation

$$f(t) = f_o + K_v n(t). \qquad (F.1)$$

Each VCO simulates the output of one track of the tape recorder on
which a sinusoid has been recorded. The instantaneous frequency of
the recorder output is obtained from (2.13).

$$f(t) = f_o + f_o g(t). \qquad (F.2)$$

Comparing (F.1) with (F.2) and substituting the values for the VCO
parameters gives

$$n(t) = -32.5 \, g(t), \qquad (F.3)$$

which establishes the desired relationship between VCO signal and
flutter. The spectrum of $n(t)$ can be shaped to give the desired
flutter spectrum.

A random noise generator was used to generate a zero-mean Gaussian
distributed noise voltage with an amplitude spectral density which is
plotted in Fig. F.2. Also shown are the frequency responses of two
filters which were used to shape the spectrum of the noise. The
flutter spectrum used in the design example was generated with Filter
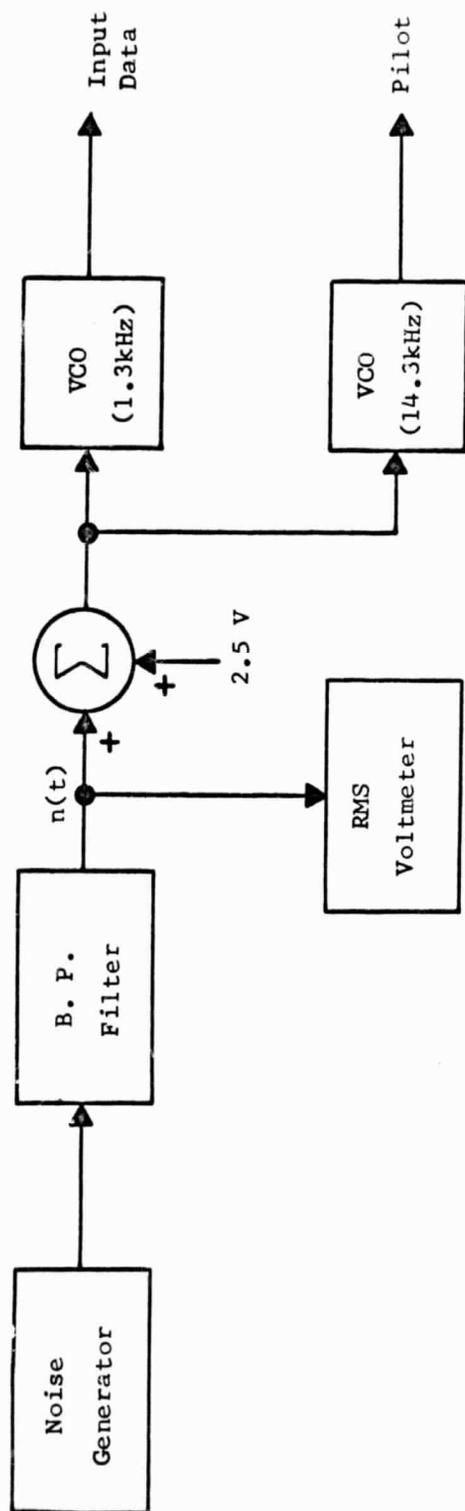1 and Filter 2 was used to generate the spectrum needed to illustrate

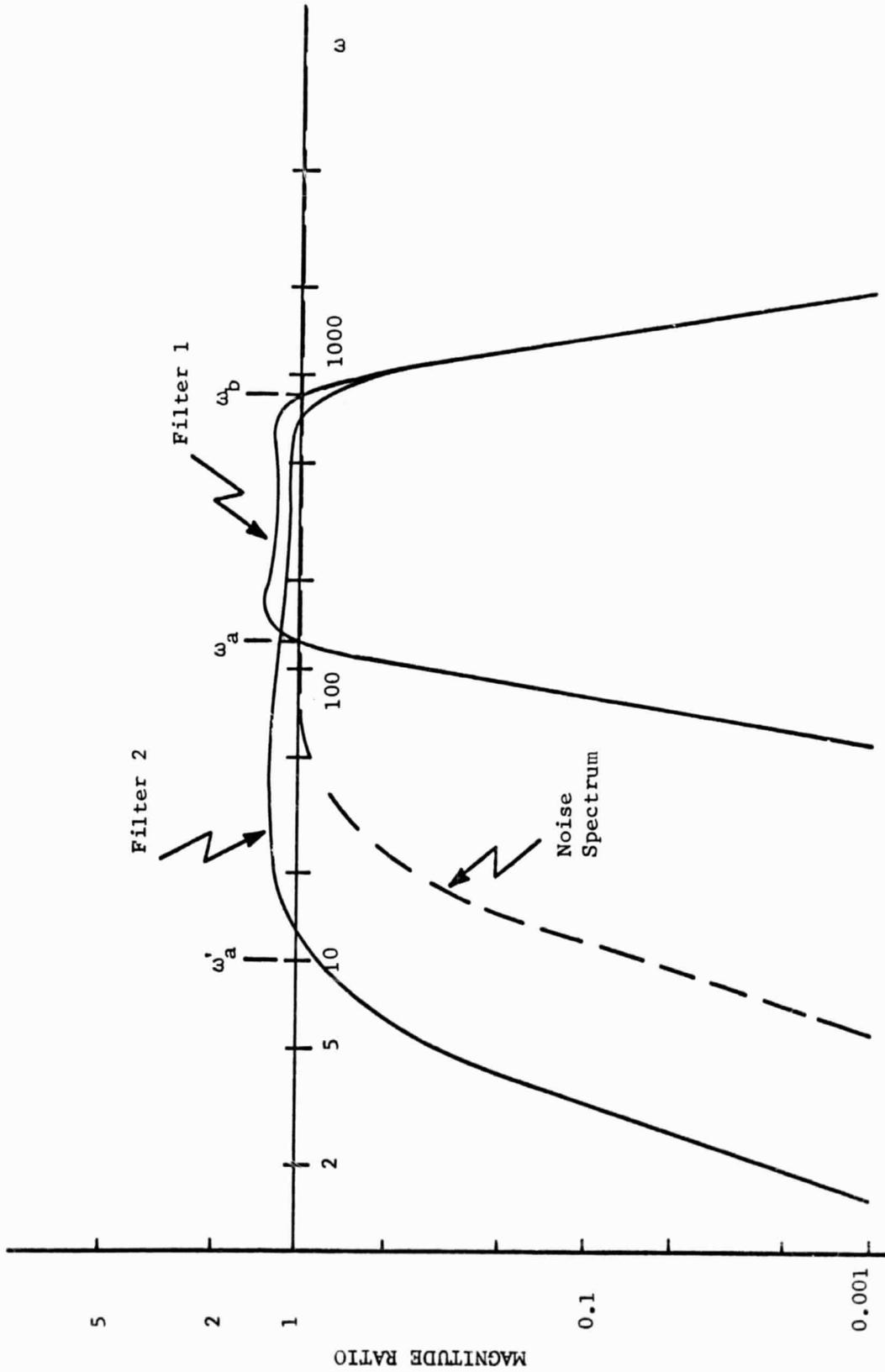Fig. F.1. Technique for Simulating Tape Recorder Signals with TBE.

84

Fig. F.2. Frequency Spectrum for Noise Generator and Amplitude Response of Two Bandpass Filters.

the effect of low-frequency flutter. The rms value, N, of $n(t)$ was determined from (F.3) by substituting the value 4.3×10^{-3} given for the rms value of $g(t)$ in the design example.

$$N = 0.14 \text{ V.} \qquad\qquad (F.4)$$

REFERENCES

1. R. S. Simpson and W. H. Tranter, "Effect of recorder time-base error on an AM-baseband telemetry system," IEEE Trans. Communication Technology, vol. COM-16, pp. 316-320, April 1968.

2. G. L. Davies, Magnetic Tape Instrumentation, New York: McGraw-Hill, 1961, pp. 137-152.

3. S. C. Chao, "Flutter and time errors in instrumentation magnetic recorders," IEEE Trans. Aerospace and Electronic Systems, vol. AES-2, pp. 214-223, March 1966.

4. R. S. Simpson and R. C. Davis, "Tape recorder analysis and bit rate smoothing of digital data," Bureau of Engineering Research, University, Alabama, Tech. Rept. 8, Contract NAS8-20172, June 1966.

5. S. C. Chao, "Time base compensation in magnetic tape recorders," Proc. IEEE (Letters), vol. 54, pp. 1572-1573, November 1966.

6. R. S. Simpson, "Tape recorder analysis and bit-rate smoothing of digital data," op. cit., pp. 5-12.

7. S. C. Chao, "The effect of flutter on a recorded sinewave," Proc. IEEE (Letters), vol. 53, pp. 726-727, July 1965.

8. S. C. Chao, "Flutter and time errors in instrumentation magnetic recorders," op. cit., p. 215.

9. R. S. Simpson, "Tape recorder analysis and bit-rate smoothing of digital data," op. cit., pp. 38-46.

10. G. L. Davies, op. cit., pp. 101-107.

11. S. C. Chao, "Time base compensation in magnetic tape recorders," op. cit., p. 1572.

12. F. J. Witt, "An experimental 224 Mb/s digital multiplexer-demultiplexer using pulse stuffing synchronization," Bell Sys. Tech. J., vol. 44, pp. 1852-1856, November 1965.

13. Digital Equipment Corporation, Digital Logic Handbook, Maynard, Massachusetts, 1968, p. 27.

14. Beckman Instruments, Inc., Beckman Electronic Instrumentation, Richmond, California, 1967/68, p. 20.

15. Engineered Electronics Company, EECoLogIC Integrated Circuit Logic Cards, Santa Ana, California, June 1966.

16. J. N. Giles, Fairchild Semiconductor Linear Integrated Circuits Applications Handbook, Fairchild Camera and Instrument Corporation, p. 174.

17. Telemetry Standards, Inter-Range Instrumentation Group, Range Commanders Council, White Sands Missile Range, New Mexico, 1966.

18. J. C. Hancock, An Introduction to the Principles of Communication Theory, New York: McGraw-Hill, 1954, p. 56.

19. J. L. Bower and P. M. Schultheiss, Introduction to the Design of Servomechanisms, New York: Wiley, 1958, pp. 162-202.

20. Ibid, p. 83.

21. H. Chestnut and R. W. Mayer, Servomechanisms and Regulating System Design, vol. 1, New York: Wiley, 1959, p. 561.

22. G. C. Newton, L. A. Gould and J. F. Kaiser, Analytical Design of Linear Feedback Controls, New York: Wiley, 1957, pp. 371-381.

23. R. S. Simpson, "Tape recorder analysis and bit-rate smoothing of digital data," op. cit., p. 52.

COMMUNICATION SYSTEMS GROUP

RECENT REPORTS

An Exponential Digital Filter for Real Time Use, R.S. Simpson, C.A. Blackwell and W.H. Tranter, July, 1965.

An Evaluation of Possible Modifications of the Existing IRIG FM/FM Telemetry Standards, R.S. Simpson, C.A. Blackwell and J.B. Cain, May, 1966.

Analysis of Premodulation Gain in a SS/FM Telemetry System, R.S. Simpson and C.A. Blackwell, June, 1966.

Tape Recorder Flutter Analysis and Bit-Rate Smoothing of Digital Data, R.S. Simpson and R.C. Davis, June, 1966.

A Study of Redundancy in Saturn Flight Data, R.S. Simpson and J.R. Haskew, August, 1966.

AM-Baseband Telemetry Systems, Vol. 1: Factors Affecting a Common Pilot System, R.S. Simpson and W.H. Tranter, February, 1968.

Waveform Distortion in an FM/FM Telemetry System, R.S. Simpson, R.C. Houts and F.D. Parsons, June, 1968.

A Digital Technique to Compensate for Time-Base Error in Magnetic Tape Recording, R.S. Simpson, R.C. Houts and D.W. Burlage, August, 1968.